EES Catalysis

PERSPECTIVE

View Article Online
View Journal | View Issue

Cite this: *EES Catal.*, 2026, 4, 642

Are plasma discharges really "catalyst-free"?

Thuy Vy Le, [a] C. Buddie Mullins [abc] and Thomas C. Underwood *[cd]

Many plasma chemistry studies assume that chemical reactions occur either within the volume of plasmas or on heterogeneous catalysts that are distributed in packed beds. This designation overlooks the catalytic role of electrodes that bound the plasma. Beyond sustaining the discharge through electron emission, electrodes can act as chemically active interfaces, undergoing erosion, film growth, and nanoparticle release that influence the reactivity of the plasma phase and surrounding surfaces or interfaces. Literature comparisons show that reactors with catalytically active electrodes often achieve similar or higher performance than packed-bed systems, while reactors with inert boundaries underperform. Here, we perform experiments using a nanosecond-pulsed spark discharge for ammonia synthesis to elucidate how electrodes contribute catalytic reactions in plasma systems. We find that electrode composition affects both yield and energy efficiency strongly: under identical discharge settings, Ni electrodes produced 0.37% NH_3, Cu 0.32%, SS 304 0.23%, and W only 0.11%, and on Cu, adjusting the feed ratio from $N_2:H_2$ = 1 : 3 to 1 : 7 increased NH_3 yield sevenfold (0.3% to 2.2%). SEM-EDX and XPS analyses confirm that plasma operation generates Cu/Cu–N nanoparticles that coat surfaces within reactors and induce electrode nitridation, providing dynamic nitrogen storage and release and establishing hidden catalytic cycles. These electrode-driven processes influence yields, selectivity, and mechanistic pathways directly. Recognizing electrodes as catalytic elements is essential for accurate mechanistic interpretation, fair benchmarking, and deliberate design of plasma systems, ensuring that advances in plasma chemistry are based on realistic assessments of surface contributions.

Received 24th October 2025,
Accepted 17th February 2026

DOI: 10.1039/d5ey00305a

rsc.li/eescatalysis

Broader context

Plasma reactors that use electrodes are often described as "catalyst-free," yet their surfaces participate actively in reactions and influence plasma chemistry. The composition and evolution of these electrodes can alter reaction mechanisms, energy transfer, and product distributions, making it essential to treat them as catalytic elements rather than inert boundaries. In this perspective, we propose a boundary-based framework that accounts for electrode effects and provides a consistent design space for comparing plasma catalyst systems. We show that electrodes in reactive plasmas evolve dynamically, they erode, form reactive films, and release nanoparticles that generate new catalytic sites, even in systems that are not intentionally designed with catalysts. To illustrate these effects, we conducted nanosecond pulsed spark discharge experiments for ammonia synthesis and observed changes in yield, nanoparticle formation, and surface nitridation on the electrodes. These results reveal that electrodes act as active catalytic interfaces that shape reaction mechanisms within plasma environments. Recognizing their role unites concepts from plasma chemistry and heterogeneous catalysis, providing a foundation for rational electrode design and improved control of plasma-driven synthesis for sustainable fuels and chemicals.

1. Introduction

Plasma catalysis offers a promising route to sustainable chemical synthesis by enabling reactions to run directly on electricity at lower temperatures and pressures than conventional thermal processes.[1–4] This approach has been demonstrated in diverse applications, including ammonia synthesis,[5–9] carbon dioxide splitting,[10,11] methane conversion,[11,12] hydrocarbon reforming, hydrogen generation,[13] air purification,[14,15] and nanomaterial production.[16,17] In these systems, non-thermal plasmas (NTPs) generate energetic electrons (~1–10 eV) that produce radicals, ions, and vibrationally excited molecules while keeping the bulk gas (the translational degree of freedom) near ambient temperature.[1,18] Such plasma-activated species lower activation barriers and allow the cleavage of strong bonds (*e.g.*, N≡N and C=O), opening reaction channels that are

[a] *Department of Chemistry, The University of Texas at Austin, Austin, TX 78712, USA*
[b] *McKetta Department of Chemical Engineering, The University of Texas at Austin, Austin, TX 78712, USA*
[c] *Texas Materials Institute, The University of Texas at Austin, Austin, TX 78712, USA. E-mail: thomas.underwood@utexas.edu*
[d] *Department of Aerospace Engineering and Engineering Mechanics, The University of Texas at Austin, Austin, TX 78712, USA*

inaccessible under mild thermal conditions.[4,5,8] When combined with heterogeneous catalysts, the plasma supplies a flux of excited species that drive chemisorption and guide intermediate formation through both Langmuir–Hinshelwood (L–H) and Eley–Rideal (E–R) mechanisms.[19,20] The properties of the catalyst, such as adsorption energies and surface temperature, then determine how intermediates recombine, influencing both product pathways and catalyst stability. Together, this coupling between plasma and catalysts expands the design space for heterogeneous catalysis, enabling control over selectivity, suppressing deactivation, and supporting the use of abundant or unconventional materials.[2,21,22] However, predicting when and where such synergies emerge, and translating them into rational design rules, remains a challenge.

Heterogeneous reactions in plasma catalytic systems span multiple length scales, adding further complexity to their behavior. In porous media and packed bed reactors, catalysts are typically dispersed on dielectric supports to increase surface area, while embedded transition metals or other catalytic phases provide active sites for bond activation. At the nanoscale, microporous structures ($\sim$10 nm) and catalytic nanoparticles set the density and accessibility of active sites where plasma-activated species react.[21–23] At mesoscopic scales ($\sim$50 μm–1 cm), interstitial voids govern transport and plasma penetration, determining which species reach reactive surfaces.[24,25] At reactor scales ($\sim$cm–m), the arrangement of beds and supports shapes the discharge and couples the bulk plasma state (*e.g.*, density, energy distribution) to surface reactions. Beyond providing binding sites, these materials influence plasma behavior directly: dielectric supports store charge, promote microdischarges, and enhance local fields, while catalytic and conductive surfaces interact with radicals, ions, and electrons in ways that reshape the discharge itself.[24,26–28] This multiscale interplay between surfaces and plasma dynamics determines both catalytic performance and reactor stability, underscoring the importance of designing systems that account for all active surfaces across scales.

However, the catalytic role of electrodes that sustain the plasma is often underreported in mechanistic terms, even though their effects have been noted for decades. Classically, these surfaces are considered as emissive elements that supply electrons to maintain plasma discharges. Chemical reactions are thought to occur volumetrically within the plasma phase where molecules are excited (*i.e.*, in streamers) or on catalytic materials that are placed between the electrodes. Electrode erosion and surface changes under plasma exposure have long been observed: early glow discharge studies showed that changing only the electrode metal shifted ammonia production rates.[29] Later work found that tangled-wire and high surface area electrodes boost yields by increasing the active interface,[30] while recent studies of dielectric barrier discharges (DBDs) have shown that electrodes shed nanoparticles that spread throughout the reactor, seeding new active sites and altering product distribution.[31] Both spark discharges and DBDs generate nanoparticles through thermal evaporation and ion sputtering at electrode surfaces, with particle size and yield depending strongly on discharge energy.[32] Ion bombardment, local heating, and reactive gases are known to wear down electrodes and change their surface chemistry, including the formation of nitrides and oxides.[16,33]

Despite this qualitative awareness, electrodes are active chemical interfaces whose mechanistic contributions are rarely quantified or controlled. Under plasma exposure, electrodes absorb and recombine reactive species, undergo sputtering, and continuously evolve as their surfaces erode. This erosion can release nanoparticles into the discharge, where they disperse and create hidden catalytic sites throughout the reactor volume. Nanoparticle formation within plasmas is well-established in dusty plasma and materials synthesis communities, where plasma-generated particles have been shown to undergo chemical transformation through interaction with reactive species in the discharge environment.[16,34,35] These findings suggest that even systems without packed-bed catalysts are rarely "catalyst-free." Instead, electrodes contribute directly through their evolving surface chemistry and indirectly by supplying new catalytic material as they degrade. Recognizing electrodes as dynamic chemical interfaces, rather than passive electrical components, reframes how plasma chemistry can be interpreted and reveals additional pathways for synergies between plasmas and catalysts across a wide range of reactions.

In this work, we seek to uncover the mechanisms by which electrodes impact plasma chemistry and bridge the gap between what is known about electrode effects and how they are reported, by proposing a framework that clearly accounts for their catalytic role. Electrode effects are rarely measured, controlled, or described in enough detail to allow comparison across studies. We introduce a boundary-based classification scheme, separating external from internal boundaries and inert from catalytic surfaces, along with a design-space framework to help researchers evaluate all active surfaces in plasma reactors, including electrodes. To support this viewpoint, we present case studies showing how electrodes in reactive plasmas evolve dynamically: they erode, form reactive films, and release nanoparticles that seed new catalytic sites, even in studies that do not consider their effect. For example, we performed experiments with nanosecond pulsed spark discharges to synthesize ammonia (NH_3) and found that the electrode material (*e.g.*, Ni, Cu, W) changed the process yield by up to 400%. On Cu electrodes, we found that by tuning the $N_2:H_2$ feed ratio from 1 : 3 to 1 : 7, the NH_3 yield increased sevenfold (from 0.3% to 2.2%), with surface analysis (SEM-EDX, XPS) confirming the formation of Cu/Cu–N nanoparticles and electrode nitridation that enabled dynamic nitrogen storage and release. These findings will be used to demonstrate that electrodes function as active catalytic elements rather than passive boundaries, and that neglecting their role can obscure mechanistic interpretation. Recognizing electrodes as integral reaction interfaces, not just emissive components, is critical to better understand plasma-driven chemical mechanisms and to design more efficient and sustainable plasma processes.

2. The plasma-catalytic design space

Plasma catalysis opens a fundamentally different design space for chemical reactions. Plasmas generate reactant molecules in

a variety of excited states, including vibrational, electronic, radical, and ionic species, that adsorb and interact with surfaces in ways that are distinct from ground-state and inert reactant molecules. By decoupling specific bond activations from catalyst properties or bulk thermal conditions, plasmas create opportunities to control selectivity and reaction pathways that are inaccessible in conventional catalysis. The plasma catalytic design space emerges from the overlap of plasma states, surface conditions, and bulk material properties, each contributing distinct factors that govern reaction kinetics and branching pathways (Fig. 1A). Plasma parameters such as electron, ion, and vibrational temperatures (T_e, T_i, T_{vib}), species densities (n_e, n_n), and energy distributions regulate the flux of radicals, ions, metastables, and excited molecules to surfaces, states that are inaccessible under purely thermal excitation at mild conditions. At the interface, properties like surface temperature (T_{sur}), roughness (R_a), and chemical condition (oxides, adsorbates, defects) control sticking, intermediate recombination, and local field enhancement. The bulk material, including supports, adds intrinsic properties, including work function (Φ), conductivity, resistivity, and thermal transport, which define thresholds for electron emission, charge balance, and heat dissipation. The next section explores how the intersection of these plasma parameters, surface states, and material properties reshapes catalytic reactions, and emphasizes the role of electrodes as active contributors.

Heterogeneous catalysis in plasmas proceeds through well-established surface mechanisms, but the discharge environment fundamentally reshapes how these mechanisms operate. The continuous flux of radicals, ions, and vibrationally or electronically excited molecules extends bond activation beyond the surface, directly coupling catalytic reactions with processes that are initiated in the plasma phase. Unlike thermal catalysis, this activation is not limited by surface adsorption energies or bulk gas properties, since plasmas sustain non-equilibrium states where internal molecular temperatures (*e.g.*, vibrational, T_{vib}) that far exceed the translational gas temperature (T_{gas}). These conditions allow the rates of individual reaction steps to be tuned independently, providing a means to break catalytic scaling relations and enable the use of less expensive materials. Plasma control has already been shown to overcome scaling laws for NH_3 synthesis and non-oxidative CH_4 conversion.[5,15,36–38] Within this framework, Langmuir–Hinshelwood steps involve co-adsorption and bond rearrangement on the surface, while Eley–Rideal steps occur when plasma-activated species collide directly with adsorbed intermediates.[39] Additional pathways, such as Langmuir–Rideal (L–R) processes where a gas-phase radical or metastable from the plasma reacts with a weakly adsorbed species before it fully equilibrates on the surface,[2,21,23] may also arise because plasma-driven fluxes lower activation barriers and open channels that are unavailable under thermal conditions. Once species adsorb, however, their non-thermal "memory" is lost

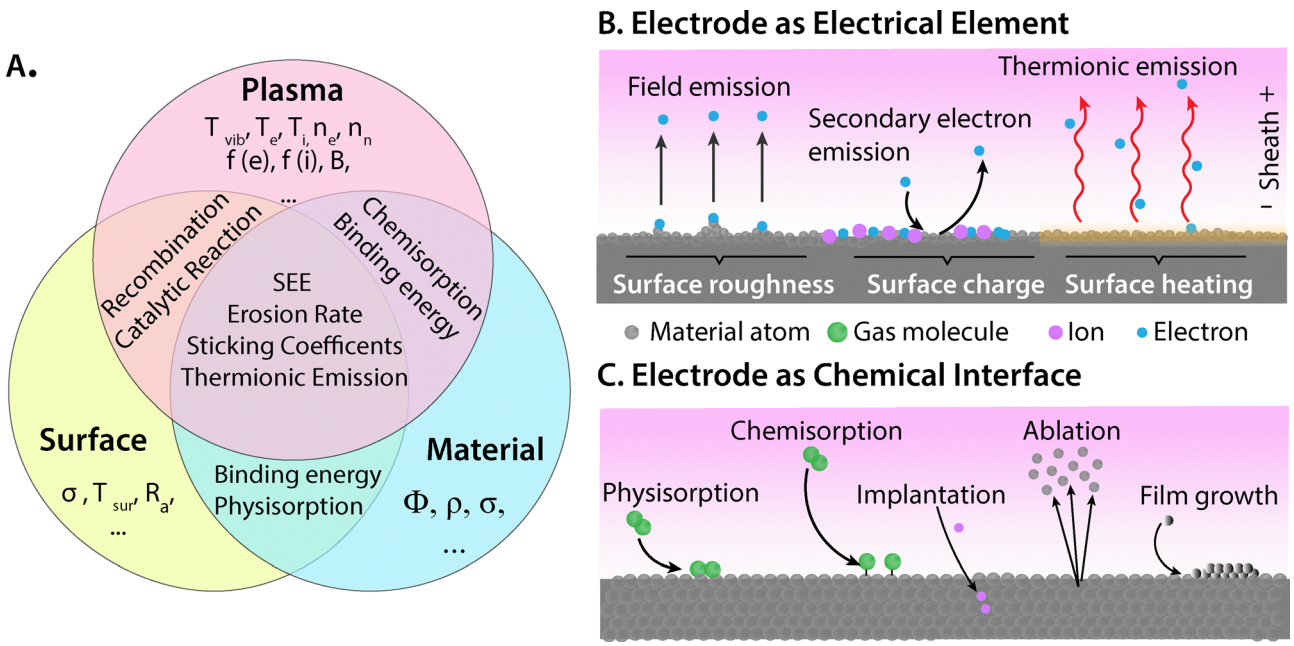

Fig. 1 Plasma catalytic design space at plasma solid interfaces. (A) A Venn diagram showing how plasma conditions, surface state, and material properties define the operational space for plasma catalysis. Plasma variables include the temperature of electrons, ions, and molecular vibrational (T_e, T_i, T_{vib}); number density of electrons, and neutral gas (n_e, n_n); distribution functions of plasma species *f* (e) and *f* (i); and magnetic field (B). Surface descriptors include stress (σ), surface temperature (T_{sur}), and roughness (R_a). Bulk material properties include work function (Φ), resistivity (ρ), and electrical conductivity (σ). Overlaps mark coupled processes, plasma–surface (recombination, catalytic reactions), plasma–material (chemisorption, binding energy), and surface–material (physisorption, binding energies, *etc.*). The center lists shared responses: secondary electron emission (SEE), erosion rate, sticking coefficients, and thermionic emission. (B) Electrodes act as emissive elements to supply electrons to sustain plasma discharges through field emission, SEE, and thermionic processes. (C) Electrodes also act as chemical interfaces where physisorption, chemisorption, implantation, ablation, and film growth can occur, linking plasma chemistry to catalytic function.

rapidly as vibrational relaxation equilibrates them with the lattice on picosecond timescales (~1–6 ps for chemisorbed species, ~10 ps for physisorbed species).[40,41] At that point, reaction pathways proceed according to surface and materials properties, governing whether intermediates recombine, transform, or desorb, rather than the non-thermal character of the plasma itself. As a result, plasmas enable outcomes that are inaccessible under purely thermal conditions, including breaking scaling relations,[5,37] altering product speciation,[1,20] increasing reaction rates,[7,42] and limiting catalytic deactivation.[15] Demonstrated examples include CH_4 conversion with coke resistance and tunable speciation,[36,38] active site regeneration,[43] and co-reactant-enabled N_2O conversion.[15] Further opportunities lie in tailoring supports, such as Al_2O_3, SiO_2, and TiO_2, where interactions between supports and active sites tune plasma-driven chemistry, and in designing complex catalysts such as bimetallic systems, which expand the design space by promoting recombination to desired products while limiting surface poisoning.

In addition to catalysts and supports, electrodes represent another class of surfaces that are present in a variety of plasma discharges that influence both chemistry and discharge behavior directly. Electrodes are not passive boundaries, they shape reactions by emitting electrons that sustain ionization processes and excite neutral species, thereby controlling how the plasma generates reactive intermediates (Fig. 1B). Each electrode is enveloped by a sheath that regulates particle and energy exchange in its vicinity. The sheath potential drop, current–voltage response, and overall plasma stability are not determined by applied voltage alone but also depend on electrode properties. The work function (Φ) sets thresholds for thermionic emission, while surface temperature (T_{sur}) influences emission intensity. Local roughness and microstructural features enhance field emission, amplifying electron fluxes, and secondary electron emission (SEE) is sensitive not only to ion energy but also to oxide coverage, contamination, or transient adsorbates. Bulk resistivity and thermal conductivity govern charge transport and heat removal, ensuring material stability under discharge conditions. These dependencies are made explicit in plasma model boundary conditions: electrodes may be fixed or operate at a floating potential depending on circuit connections, electron flux balances include SEE and thermionic terms, and ion energies reflect sheath potential drops. By controlling electron energy distributions near the wall, electrodes determine which neutral processes receive energy from the electrical discharge, vibrational excitation at low mean electron energies, dissociation at moderate energies, or ionization at higher energies. For CH_4, for instance, electrons at different kinetic energies drive vibrational pumping (fundamental modes at 0.16–0.37 eV; efficient excitation occurs in the ~1–3 eV range), fragment generation (CH_3, CH_2, H) once dissociation channels open above ~9 eV, and ultimately ionization near 12.6 eV,[44] supplying the reactive species that feed into L–H and E–R processes. In this sense, electrodes function as active electrical boundaries that co-determine how energy is partitioned into neutral molecules close to surfaces. Vibrational excitation modes, in particular, provide favorable lifetimes (*via V–T* relaxation) and are energy-efficient compared to dissociative chemisorption barriers on catalysts, while radical-driven reactions represent more energy-expensive alternatives.[40] These electrode-dependent electrical effects have direct implications for plasma chemistry. Differences in work function and secondary electron emission coefficients between electrode materials can alter electron energy distributions, radical production rates, and sheath potentials even when external discharge settings are held constant. Simulations demonstrate that secondary electron emission, which varies with both material identity and surface condition, can shift discharges between different operating modes, dramatically altering plasma density and electron heating dynamics.[45] Similarly, particle-in-cell simulations have shown that electrode surface roughness modifies local field enhancement and electron emission characteristics, further coupling electrode condition to plasma behavior.[46] As a result, changing the electrode material may simultaneously change both the plasma state and the surface chemistry, making it difficult to fully separate these contributions without *in situ* plasma diagnostics. For studies seeking to decouple electrode-driven plasma effects from surface catalytic contributions, diagnostics that quantify radical densities and electron temperatures near electrode surfaces are essential.

Electrode polarity introduces a further asymmetry in plasma–surface interactions. In DC and pulsed DC discharges, the cathode sheath develops a substantial potential drop (cathode fall), accelerating positive ions toward the cathode with energies sufficient to drive sputtering, secondary electron emission, localized heating, and implantation of reactive species.[18] The anode sheath has a comparatively small potential drop and primarily collects electrons, resulting in less intense surface modification dominated by radical and metastable interactions rather than energetic ion bombardment. This asymmetry is well established in plasma processing: plasma nitriding specifically places workpieces at the cathode to maximize ion-driven nitrogen incorporation.[47] Corona discharge studies further demonstrate polarity-dependent behavior, with positive coronas generating streamer-based plasmas and negative coronas producing more diffuse discharges.[13,48] These differences imply that anodes and cathodes may contribute to plasma-catalyzed reactions through distinct mechanisms, an effect that remains under characterized but may significantly influence both mechanistic interpretation and reactor optimization.

Beyond their electrical role, electrodes also act as chemical interfaces that evolve continuously under plasma exposure (Fig. 1C). Classical discharge physics often treats electrodes as inert boundaries, and many "catalyst-free" studies emphasize gas phase chemistry.[49–57] For example, numerous studies model plasma chemical processes as volumetric production while neglecting catalytic boundary conditions on electrodes.[46,58–60] In reality, radicals, ions, and vibrationally excited molecules transported to electrode surfaces undergo adsorption, desorption, or recombination, with probabilities governed by surface temperature, roughness, and chemical state. Chemisorption binds reactive intermediates according to the metal's d-band structure, while physisorption stabilizes metastable species that may later desorb

or react. Ion bombardment, influenced by the surface polarity, generates defects such as vacancies, adatoms, and step edges, which act as preferential adsorption sites with altered binding energies. These impacts can also implant atoms into subsurface layers, forming interstitial species or new phases that modify the surface's catalytic activity. Simultaneously, sputtering, ablation, or micro-melting releases metal atoms and nanoparticles into the plasma. These species can act as hidden catalysts through gas-phase reactions, redeposit to form catalytic films on reactor walls and internal surfaces, or be distributed into liquid phases in plasma-electrochemical systems, complicating the mechanistic interpretation of product formation. This dynamic behavior generates an extended catalytic network throughout the reactor that originates from electrodes but extends beyond their geometric boundaries. Electrode surfaces also undergo phase transformations under reactive plasmas: nitrogen plasmas produce metal nitrides, oxygen-containing discharges form oxides, and hydrocarbon environments generate carbides. These phases exhibit different catalytic properties than the parent metal, thereby affecting reaction selectivity and activity.

Importantly, the catalytic properties of these transformed phases differ substantially from those of the parent metal. Nanoparticles ejected from electrodes undergo compositional changes as they transit through the plasma, reacting with activated species to form nitrides, oxides, or carbides depending on the gas environment. These transformed nanoparticles then redeposit throughout the reactor with altered catalytic properties that affect reaction yields. For example, copper nanoparticles generated in nitrogen-containing plasmas may partially convert to Cu_3N, which has different nitrogen binding characteristics than metallic Cu. The catalytic activity of the system thus depends not only on the initial electrode material but also on the plasma-induced phase transformations that occur both at the electrode surface and on dispersed nanoparticles.

Erosion, redeposition, defect formation, and phase transformation cause electrode surfaces to evolve continuously during plasma operation. Consequently, electrodes function as dynamic boundaries that participate actively in plasma chemistry, including surface catalytic reactions that influence both reaction yields and product selectivity. Their combined electrical and chemical roles have important practical and mechanistic implications, shaping where reactions occur, how products form, and how the chemistry of a catalytic bed can be optimized to achieve desired outcomes. Despite this, the catalytic effects of electrodes remain largely overlooked in literature. Gaining mechanistic insight into electrode catalysis provides opportunities to control plasma chemistry and reaction pathways. However, to make these contributions explicit and enable meaningful comparisons across reactors, a systematic classification based on catalytic surface location is essential, as discussed in the following section.

Beyond electrode and catalyst effects, numerous other factors contribute to the variability observed in plasmacatalysis literature. Reactor geometry plays a central role: discharge gap dimensions directly influence electric field strength and plasma uniformity, while discharge length affects residence time and conversion efficiency.[61] In packed-bed systems, plasma penetration depth limits how much of the catalyst bed participates in reactions-typically only the first ~1 mm near the electrodes experiences significant plasma exposure.[58] Pulse parameters such as frequency, rise time, and pulse width strongly affect electron energy distributions and radical production rates, with nanosecond pulses enabling distinct reaction pathways compared to AC-driven discharges.[62] The dielectric properties of packing materials determine discharge modes and microdischarge distributions, with transitions from surface discharges to filamentary discharges occurring as dielectric constants increase.[63] Finally, feed gas composition and impurities, including trace humidity, can alter plasma chemistry by introducing additional reaction pathways involving OH radicals and other oxygen-containing species.[64] These factors often interact in complex ways, making systematic comparisons across studies challenging and highlighting the need for standardized reporting of operating conditions alongside electrode specifications.

3. Classifying plasmas in chemical synthesis

The impact of electrodes on catalysis in plasma systems depends on both the type of discharge and the reactor geometry. In plasma reactors, boundaries define the interfaces between the plasma and solid surfaces, constraining plasma properties, physics, and chemistry through boundary conditions. These boundaries can be classified as external boundaries (EB) or internal boundaries (IB) (Fig. 2A), based on their location within the plasma. External boundaries are the surfaces that confine the plasma at its outer edges, typically including reactor walls, dielectric barriers, or electrodes that sustain the discharge. Internal boundaries, by contrast, include any solid objects placed within the active plasma zone, such as pellets, packed-bed catalysts, or inserted electrodes. Within this framework, plasmas can be broadly categorized as contact (electrodes in direct contact with the plasma) or contactless (plasma forms without direct electrode contact) schemes. This classification provides a systematic way to identify where plasma-solid interactions occur and whether these interfaces participate actively in chemical transformations across different forms of plasma catalysis. The classification framework presented here complements the conventional system that is widely used in the plasma catalysis literature, which distinguishes configurations based on catalyst placement relative to the discharge zone.[1,21] The existing classification system categorizes reactors as: (1) plasma-only, where no intentional catalyst is present; (2) in-plasma catalysis (IPC), where catalyst material is placed directly within the discharge region; and (3) post-plasma catalysis (PPC), where catalyst is positioned downstream of the plasma. By focusing on which surfaces contact the plasma regardless of intent, our EB/IB framework captures catalytic contributions from electrodes in systems designated as "plasma-only", contributions that would otherwise be overlooked.

Three distinct cases arise when considering the catalytic nature of plasma reactor boundaries: inert EBs, catalytic EBs,

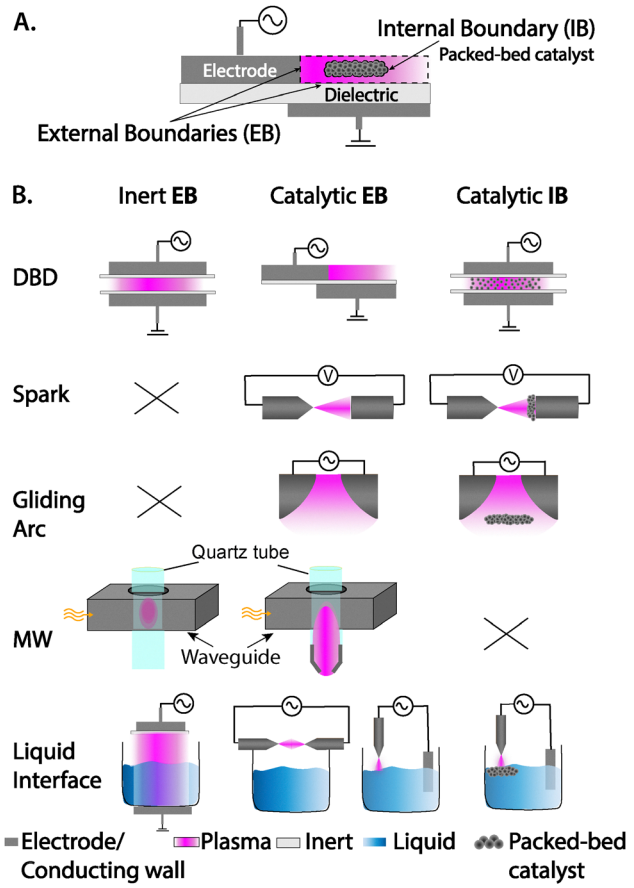

Fig. 2 Classification of plasma reactors by boundary type and catalyst placement. (A) Schematic illustration of external boundaries (EB) and internal boundaries (IB) in a plasma discharge. EB represents the reactor walls and electrodes, which can be inert or catalytic. IB refers to solid materials present inside the discharge region, such as packed-bed catalysts. (B) Plasma sources categorized based on boundary and catalyst configuration. Rows are organized from top to bottom as follows: dielectric barrier discharge (DBD), spark, gliding arc, microwave (MW), and plasma–liquid interface. Columns arranged from left to right include inert EB, which consists of inert material; catalytic EB, which features electrodes or conductive walls; and catalytic IB, where the catalyst is placed directly in the discharge as a packed bed or particles. "*x*" indicates combinations that are uncommon.

and catalytic IBs. Inert EB systems employ non-catalytic materials, such as quartz, ceramic, or certain phases of Al_2O_3, to confine the plasma without contributing catalytic reactions on surfaces that change the product speciation in a chemical process. These represent true catalyst-free discharges, where catalysis at the boundaries is negligible. Catalytic EB systems, in contrast, use boundary materials that themselves act as catalysts, most commonly catalytic electrodes. These surfaces offer adsorption sites, facilitate dissociation of stable molecules such as N_2 and CO_2 and stabilize plasma-generated radicals. Despite these roles, EB are often commonly not recognized as catalysts because they are integrated into the reactor hardware, leading to underestimation of their effects on reaction yields and energy efficiency, which may be misattributed to "plasma-only" effects. Catalytic IB systems introduce the catalyst directly into the plasma, as in packed-bed or monolithic configurations, where for example transition-metal sites (Ni, Cu, Fe, Ru) on oxide supports interact with plasma-activated species. Post-plasma catalytic configurations place packed beds outside the plasma but within transport lifetimes so that reactive species generated in the plasma can still interact with surfaces and contribute to catalytic reactions.[65] The presence of catalytic IB within plasmas adds multiscale complexity, generating microscale plasma regions in pores, modifying mesoscale transport through porous networks, and influencing macroscale discharge stability.[25,28,58]

These descriptors can be used to categorize existing plasma reactor designs, each exhibiting distinct electrode arrangements and discharge characteristics. Dielectric barrier discharges form plasmas along dielectric surfaces between electrodes, where at least one electrode is covered by a dielectric material. Streamers propagate along the dielectric surfaces in these discharges or between exposed electrodes and the dielectric, driving localized plasma chemistry. Fully insulated electrodes create DBDs in an inert EB configuration, while exposed catalytically active electrodes (*i.e.*, asymmetric designs)[66] yield catalytic EBs. Spark discharges generate transient (~ns), high-voltage discharges between exposed metal electrode tips, often producing surface ablation and localized heating on the electrodes. Gliding arcs (GAs) create flow-stabilized, steady-state arcs that travel along diverging electrodes with the gas flow. Their non-equilibrium character arises from rapid arc elongation by gas flow, which cools the arc column faster than equilibrium can be established. This creates a unique regime where electron temperatures reach 1–2 eV while gas (translational) temperature remains below 3000 K, enabling efficient vibrational excitation and selective chemistry not achievable in thermal arcs.[65] Spark and gliding arc discharges operate as catalytic EB systems because metal electrodes are needed to maintain the discharge. Microwave (MW) plasmas, like other RF contactless discharges (*e.g.*, inductive plasmas), use directed electromagnetic waves to induce gaseous breakdown within cavities, eliminating the need for direct contact between electrodes and the plasma. Microwave reactors function with inert EBs typically depending on how far away the cavity walls are from the discharge. Plasma-liquid systems couple discharges to electrode and liquid interfaces, typically forming catalytic EB configurations, common modes include post-plasma (post-discharge) treatment of liquids or plasma-activated water produced upstream,[67] glow-discharge electrolysis where a gas-sheath discharge forms above the liquid,[68] and contact glow-discharge electrolysis (also called plasma-driven solution electrolysis) where a luminous plasma envelope forms directly around a submerged electrode.[68] Despite these differences in power sources and geometries, all of these configurations share a common feature: the plasma interacts with boundaries that influence discharge properties and chemistry. Fig. 2B maps each configuration onto the EB/IB framework, with X marks highlighting combinations that are uncommon due to practical constraints in reactor design and discharge physics.

When packed beds, monoliths, catalyst coatings, or electrodes are added to suitable setups, the system gains catalytic IB

reactions, but an important limitation reduces their effectiveness. Computer modeling by Van Laer and Bogaerts shows that plasmas penetrate packed beds only ~1 mm deep, meaning 90% or more of typical packed catalysts operate in dead zones while electrodes experience efficient coupling to the plasma phase.[58] Zhang *et al.* showed that plasmas only enter catalyst pores larger than the Debye length, further limiting the effective catalytic volume.[25] This penetration limit explains a curious observation: catalytic EB systems often match or beat the performance of complex packed-bed reactors despite having much less surface area and active sites. Consistent with this, a recent study of CH_4–CO_2 plasmacatalysis[43] reports that bare γ-Al_2O_3 often achieves 8–10% methanol selectivity, comparable to Ni/Al_2O_3 (7–9%) and Cu/SiO_2 (6–8%), showing that many metal-loaded beds add little under plasma conditions.[69–72] The electrodes succeed through position rather than size, operating where domain overlap is strongest while packed catalysts function in regions with reduced coupling with plasmas.

4. Electrodes as catalysts in plasma systems

The classification framework can also be applied to identify trends in the literature, revealing where catalytic effects may arise and whether they were considered. Plasma chemistry studies often distinguish between "plasma" and "plasmacatalysis", yet this boundary becomes blurred when electrodes or other catalytic surfaces interact directly with the plasma. For example, while publications on plasma chemistry and plasma catalysis have grown rapidly since the 1980s (Fig. 3A, Web of Science, SI Section 2.1), a large share continue to report "plasma chemistry" without mentioning catalysts, including in detailed reaction mechanisms. In 2024 alone, over 2000 articles on plasma chemistry were published, yet only about 500 referred to catalysis explicitly. Many of these studies nonetheless relied on electrodes in direct contact with plasmas. Overlooking this distinction complicates the interpretation of plasma chemical processes, including the validation of reaction mechanisms and the optimization of plasma conditions (Fig. S1B).

We analyzed several decades of plasmacatalysis reports on NH_3 synthesis, CO_2 splitting, and CH_4 partial oxidation to determine whether catalytic EBs were described or if an effect could be inferred from reaction conditions that were used (Fig. S2C). Each study was classified using the three boundary frameworks: inert external boundaries, catalytic external boundaries, or catalytic internal boundaries. Performance metrics were converted to common units of yield or conversion *versus* specific energy input (SEI), with efficiency metrics[104] included to assess how effectively each system converted electrical energy into desired chemical products (SI Section 2.2). This standardization enables direct comparisons across reactor types and provides insight into the catalytic role of electrodes (Fig. 3B and C).

Analysis of these standardized datasets reveals that electrode material has a significant impact on ammonia synthesis (Fig. 3). As early as 1983, Yin and Venugopalan demonstrated that changing the electrode material in a glow discharge, without adding any packing, showed significant shifts in ammonia production rates.[29] This was early evidence that electrodes could do more than simply sustain a plasma. The full extent of electrode catalysis becomes clear in Fig. 3B, where catalytic EB systems achieve production efficiencies (η_f) from 0.1% to 10% – the same range as packed-bed catalysts. Among these many data points, several studies illustrate how electrode design affects performance. Iwamoto *et al.* (2017) used "wool-like" electrodes made from Au, Pt, Pd, or Cu.[6] These high-surface-area metal electrodes not only sustained the discharge but also served as active catalytic sites, yielding significant amounts of ammonia at atmospheric pressure. Ma *et al.* achieved similar success in a DBD setup by replacing simple

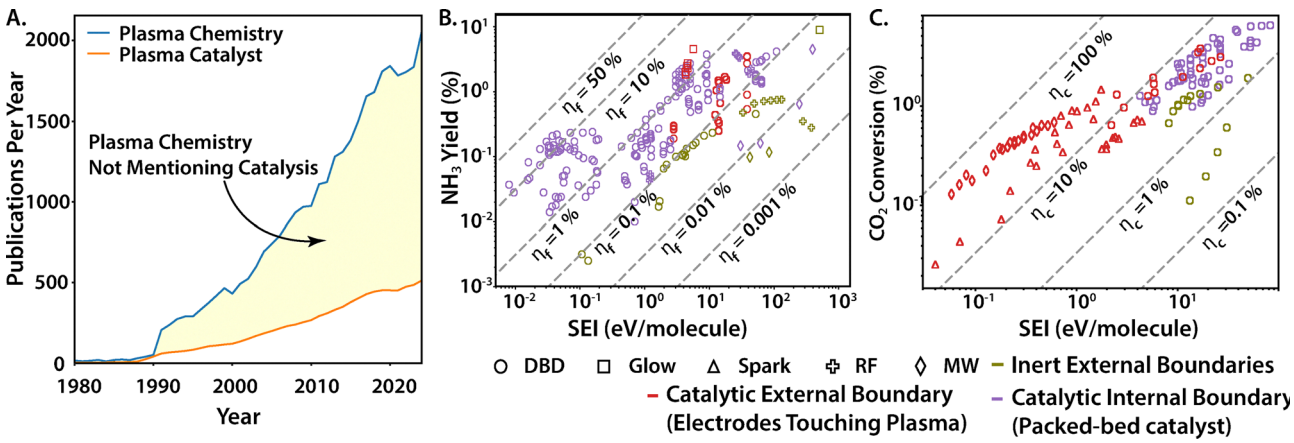

Fig. 3 Literature growth and performance in plasma catalysis (A) Annual publications (1980–2024) on plasma chemistry and plasma catalysis (search queries in SI S.2.1). The shaded region highlights the large share of plasmachemistry papers that do not mention a catalyst. (B) Normalized NH_3 yield vs specific energy input (SEI) from literature data, classified by reactor boundary type. Catalytic EB[6,29,30,73,74] perform comparably to catalytic IB,[7,9,42,73,75–86] while inert EB[19,42,73,79] yield lower performance. (C) Normalized CO_2 conversion vs SEI, showing the same trend: catalytic EB[87–94] and catalytic IB[27,58,95–102] reactors overlap in performance space, while inert EB[27,96,97,99,101–103] systems underperform. All plots were generated by the authors from reported values in the cited references.

rod electrodes with a tangled-wire electrode, which increased the available metal surface area.[30] This modification boosted ammonia concentration and reduced energy cost, directly linking electrode morphology to catalytic efficiency.

Studies involving CO_2 conversion reveal the same hidden electrode effects across numerous investigations. In Fig. 3C, catalytic EB systems achieve conversion efficiencies (η_c) above 5%, matching and sometimes surpassing packed-bed reactor performance. Early DBD studies by Aerts *et al.* showed that significant CO_2 conversion could be achieved without any catalyst packing, simply by tuning discharge parameters such as gap size and SEI.[87] They found energy input was the dominant factor controlling both conversion and efficiency. More recently, Yong and colleagues reported that a nanosecond-pulsed plasma operating at elevated pressure achieved ~14% CO_2 conversion with 20–23% energy efficiency, performance comparable to many plasma catalyst systems.[94] Surprisingly, adding catalyst pellets to DBD reactors often yielded only modest gains, improving efficiency by just a few percent rather than transforming performance. This suggests metal electrodes already catalyze key steps, including dissociative adsorption of CO_2 and oxygen atom recombination. Vibrationally excited CO_2 also interacts with electrode sites, lowering bond-breaking barriers. Electrode sputtering releases metal nanoparticles that become floating catalysts in the discharge. Thus, what seems like "plasma-only" processing actually involves both plasma and electrode catalysis. CH_4 partial oxidation (Fig. S1C) shows identical patterns.

Together, these data demonstrate that electrodes act as active catalysts across a wide range of plasma-driven reactions. However, the rapid growth of publications, coupled with incomplete reporting of electrode details, has resulted in many studies overlooking their catalytic role. Treating electrodes as chemically reactive interfaces not only deepens mechanistic insight into plasma environments but also reveals opportunities to enhance process performance.

5. Case study – nanosecond pulse spark discharge for NH_3 synthesis

Controlled experiments were performed to demonstrate the mechanisms by which electrodes act as catalytic participants in plasma chemistry. Nanosecond-pulsed spark discharges in a pin-to-pin configuration were selected as a model system because plasma is sustained directly between metallic tips (*i.e.*, catalytic EBs). In this configuration, electrodes experience intense fields, ion bombardment, and ablation, allowing them to serve simultaneously as sources of electron emission and catalytic active sites. Ammonia synthesis was chosen as the representative reaction because its surface-driven mechanism is well characterized, highly sensitive to catalytic composition, and directly illustrates how nitrogen activation couples into surface-driven catalytic pathways. Under spark conditions, ablation injects nanoparticles and alters surface phases, creating a dynamic catalytic interface that continuously reshapes plasma chemistry. By varying electrode composition systematically under identical discharge settings, these experiments isolate surface-driven mechanisms, track ablation-induced effects, and connect them to performance in plasma-driven ammonia synthesis.

5.1. Reactor design and plasma overview

The reactor used in this study is a compact flow cell designed to operate with nanosecond-pulsed spark discharges at ambient pressure (Fig. 4A). Two electrodes face each other in a pin-to-pin configuration across a narrow 3 mm gap: one is flat, while the other is sharpened to concentrate the electric field and reliably ignite sparks.[12] A premixed N_2/H_2 feed, controlled between 1.2 and 8 sccm (details in SI Section 1), passed through the gap where high-voltage pulses of 8 kV, current at ~4 A and 200 ns duration are applied at 3 kHz frequency. These short, high-voltage bursts allowed stable operation while keeping the bulk gas near room temperature, ensuring that most of the supplied energy was directed into the plasma to drive chemical reactions.

A nanosecond spark forms an intense, localized channel between the electrodes. Because the pulse lasts only a few hundred nanoseconds, the discharge develops and quenches before the surrounding bulk gas can heat appreciably. This converts electrical energy into high-energy electrons, which drive electronic and vibrational excitation, ionization, and partial bond breaking in the N_2/H_2 mixture. Each spark thus generates a dense burst of excited N_2 molecules, N radicals, and

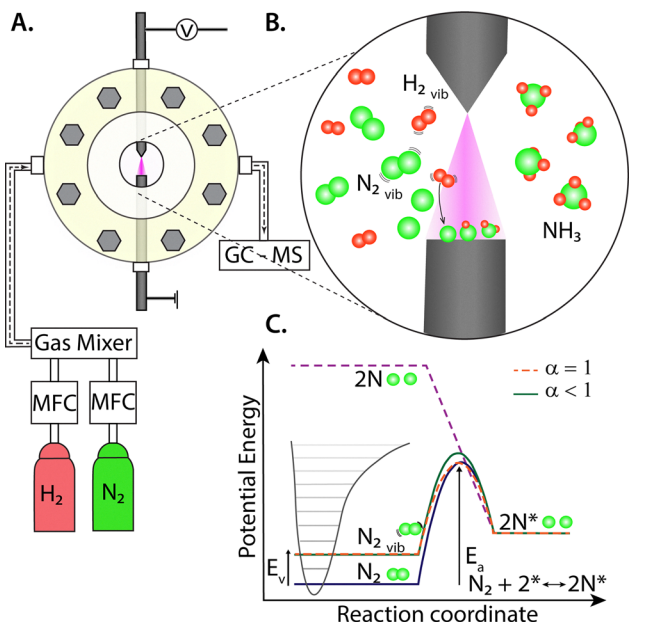

Fig. 4 Nanosecond pulsed spark discharge reactor for ammonia synthesis. (A) Reactor with flat and shaped electrodes, operated at ambient pressure with N_2/H_2 fluxes (1.2–8 sccm), ~8 kV, 200 ns pulses at 3 kHz. (B) Plasma-driven NH_3 production pathway illustration. Sparks generate energetic electrons that dissociate N_2 and H_2, forming reactive $N^\bullet$ and $H^\bullet$ species that combine through radical-mediated steps to produce NH_3 in near-ambient conditions. (C) Reaction coordinate diagram for N_2 dissociation at a surface. Showing how vibrational excitation ($N_2(v)$) raises the molecular energy and lowers the effective barrier to bond breaking.

H radicals. The electrodes play a critical role in this process because they provide the current required to sustain the discharge and shape the strong local electric fields that determine the electron-energy distribution and activation efficiency.

This transient but highly energetic environment is especially effective at activating nitrogen. High-energy electrons collide with N_2, driving vibrational excitation and even direct dissociation of the N≡N bond. On a potential-energy diagram (Fig. 4C), ground-state N_2 (0 eV) must overcome a steep dissociation barrier of ~9.8 eV to dissociate on a surface.[105] Vibrationally excited N_2 ($N_2(v)$) begins at a higher energy level, with the first few quanta adding 0.29 eV (v = 1), 0.57 eV (v = 2), and 0.85 eV (v = 3) above the ground level, which lowers the effective dissociation barrier. The Fridman–Macheret parameter (α)[65] is used to capture this effect: it reflects the fraction of vibrational energy that contributes to barrier crossing. As α increases, the apparent activation energy decreases, making dissociative adsorption more favorable. In addition, electron-impact dissociation releases atomic N radicals ($N^{\bullet}$), each ~4.9 eV above N_2, bypassing molecular activation altogether. Once generated, activated species cross the sheath and adsorb on the electrode. This sequence, plasma activation followed by transport, raises the adsorption rate constant for a fixed catalyst because species arrive pre-energized or dissociated. Adsorbates thermalize with the surface within 1–10 ps of binding,[40,41] and the chemistry thereafter follows normal surface kinetics.

From this point forward, the catalytic surface determines all recombination paths. Both Langmuir–Hinshelwood and Eley–Rideal couplings are possible. The L–H pathway involves sequential hydrogenation of adsorbed N atoms through N–H abstraction steps ($N^* + H^* \rightarrow NH^*$, $NH^* + H^* \rightarrow NH_2^*$, $NH_2^* + H^* \rightarrow NH_3$). The E–R route involves direct reactions between plasma-derived radicals in the gas phase and adsorbates, such as $N(g) + H^* \rightarrow NH^*$. This E–R channel, which complements the classical L–H hydrogenation cycle, is thought to be important in nanosecond discharges due to their large radical populations.[5] Adsorbed nitrogen atoms may recombine and desorb as N_2 if the surface binds nitrogen too weakly, potentially wasting active nitrogen. Plasma excitation speeds up adsorption, but the electrode surface's catalytic characteristics predominantly determine the final product selectivity (*e.g.*, recombination to N_2, hydrogenation to NH_3 or surface nitridation). Importantly, plasma–surface interactions can also enhance desorption. Gas-phase radicals or excited species may impinge on adsorbates and abstract them through L–R processes, forming volatile products that leave the surface. Physical energy transfer from vibrationally or electronically excited molecules can also induce non-thermal desorption by imparting sufficient energy to break adsorbate-surface bonds. Additionally, ion bombardment can sputter adsorbed species or etch surface films. These desorption pathways can "clean" surfaces that would otherwise remain saturated, freeing active sites for subsequent reactions. For ammonia synthesis under our conditions, the dominant plasma effect is enhanced nitrogen uptake; however, in other applications, such as plasma-assisted coke removal for catalyst regeneration[106] or CO_2 desorption from sorbents,[107] plasma-enhanced desorption is the primary mechanism. Thus, plasma activation can modify both adsorption and desorption rates depending on the specific system, but catalyst identity governs the critical recombination steps that set selectivity and yield.[5,7,8,20]

In this way, the nanosecond spark discharge provides a well-defined testbed: it strongly involves the electrodes, couples energy efficiently into N_2/H_2 activation, and generates the reactive species needed to overcome the intrinsic barriers of nitrogen chemistry. These features make it a great platform to directly observe how electrode materials participate in ammonia synthesis and to connect plasma activation with electrode-driven catalysis.

5.2. Evidence of catalytic effects from electrodes

Comparative experiments with Ni, Cu, SS and W electrodes were performed to reveal how strongly electrode composition controls performance in plasma ammonia synthesis. Under identical discharge settings: the same electrode gap, plasma current, and pulse conditions, the four electrode materials produced strikingly different results. At an $N_2:H_2$ ratio of 1:3, and SEI 34.5 eV molecule^{-1}, Ni electrodes consistently showed the highest NH_3 yield, reaching 0.37%, while Cu electrodes delivered intermediate performance of 0.32%, SS 304 produced 0.23% and W remained lowest at 0.11% (Fig. 5A). The corresponding N_2 conversion values followed the same order (Ni > Cu > SS 304 > W; Fig. 5B). These differences are well beyond measurement uncertainty and cannot be explained by discharged power density alone, which was held constant. Instead, they demonstrate that electrodes are chemically active boundaries that directly govern efficiency. These differences reflect catalytic scaling relations. Nitrogen binding energies follow W ≫ Ni > Cu, with W binding strongly (−2.5 to −3.0 eV), Ni near the volcano optimum (−0.5 to −0.7 eV), and Cu weakly (−0.1 to −0.3 eV).[108] SS 304 contains ~70% Fe near the volcano peak, though alloying effects may limit its activity. Under thermal conditions, weak-binding metals like Cu are inactive because N_2 dissociation is rate-limiting; however, Mehta *et al.* predicted that plasma bypasses this barrier, shifting the rate-limiting step to hydrogenation and making plasma enhancement greatest on weak-binding metals.[5] Our observed ranking (Ni > Cu > SS > W) is aligns with this prediction: when plasma supplies activated nitrogen, Cu approaches Ni performance because the dissociation bottleneck is bypassed, while W remains limited by strong N-surface interactions that trap intermediates regardless of plasma activation. We note that while external operating conditions (reactor geometry, electrode gap, pulse parameters, and flow rates) were held constant across all electrode materials, the plasma state itself, including electron energy distribution, radical densities, and sheath structure, may vary with electrode composition. Electrodes serve as boundary conditions in plasma systems, and changing the electrode material can alter the plasma properties that couple to surface reactions. The observed differences in yield therefore reflect the combined effect of electrode-dependent plasma generation and surface catalysis, both of which are influenced by electrode identity.

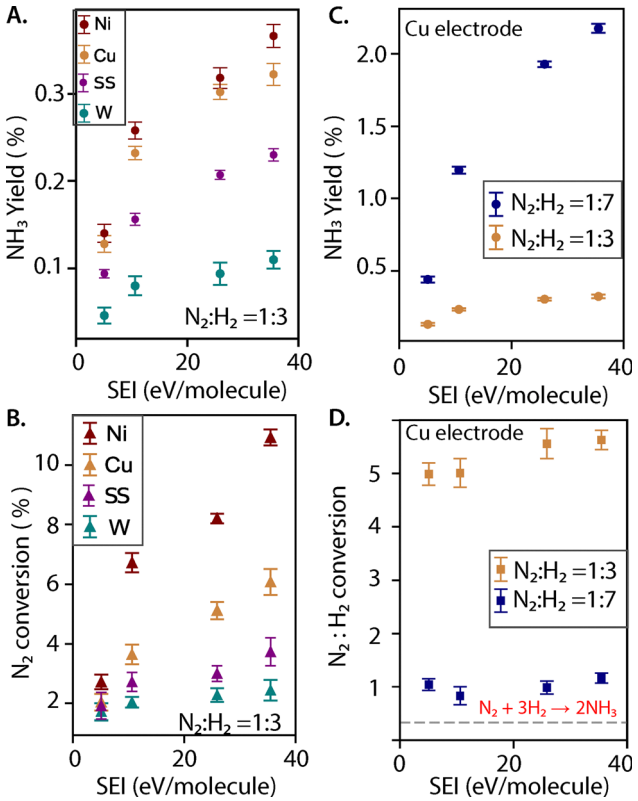

Fig. 5 Effect of electrode material and feed composition on plasma NH_3 synthesis. (A) NH_3 yield SEI for Ni, Cu, and W electrodes at a fixed $N_2:H_2$ ratio of 1:3. Ni delivers the highest yield, Cu is intermediate, and W the lowest, despite identical discharge conditions. (B) Corresponding N_2 conversion follows the same order. (C) On Cu, changing feed composition from $N_2:H_2$ = 1:3 to 1:7 produces a strong enhancement in NH_3 yield (D) $N_2:H_2$ conversion ratios exceed the stoichiometric 1:3 requirement (gray dash line), especially in N_2 rich feeds, consistent with electrode nitridation and direct nitrogen incorporation into the metal surface.

Spatially resolved optical emission spectroscopy comparing electrode materials would help deconvolute these contributions and is a target for future work.

The effect of feed composition is particularly noticeable on Cu electrodes. When the gas ratio was shifted from $N_2:H_2$ = 1:3 to 1:7, the NH_3 yield increased, from 0.3% to 2.2%, at 34.5 eV molecule^{-1} (Fig. 5C). The corresponding N_2 conversion nearly doubled as well, whereas nickel and tungsten electrodes showed much smaller composition-dependent responses. This disproportionate enhancement on Cu indicates strong composition-electrode coupling under nitrogen-rich feeds, Cu surfaces can stabilize dissociated nitrogen and promote hydrogenation more effectively than under H_2-rich conditions. For ammonia synthesis, the stoichiometric N_2/H_2 consumption to synthesize NH_3 is 1:3. In Fig. 5D, the apparent measured N_2/H_2 conversion is consistently higher than this limit (*i.e.*, 1:3); about 0.8–1.2 for the 1:7 feed and as high as 5–5.7 for the case of 1:3 N_2/H_2 flow rates. In other words, nitrogen is consumed at rates three to nearly eighteen times above what stoichiometry would predict, with the effect most pronounced when the feed is richer in N_2. Combined with the elevated N_2 conversions shown in Fig. 5B, this points to an extra nitrogen reservoir at play. Experiments were performed to prove that nitrogen was being sequestered onto surfaces as a nitride film. This behavior reinforces the broader point that electrodes in so-called "catalyst-free" plasmas are not passive, they act as reactive interfaces. Taken together, these results demonstrate that electrodes are active participants in chemistry. Changing the electrode material or the gas composition significantly alters both NH_3 yield and conversion balance, while the persistent nitrogen excess signals surface storage. The N_2/H_2 conversion ratio showed no systematic drift over hours of testing, indicating that steady-state conditions are maintained during extended operation. This stability reflects the self-renewing nature of the electrode surface: continuous ablation removes nitrided layers and exposes fresh metallic Cu, while nanoparticle generation distributes catalytic material throughout the reactor. The coexistence of metallic Cu and Cu–N phases in post-mortem XPS analysis supports this dynamic equilibrium between nitride formation and erosion.

5.3 Catalytic nanoparticle production from electrodes in plasmas

SEM-EDX was used to examine electrodes and plasma-generated particles, revealing erosion and nitrogen incorporation consistent with electrodes as active catalytic boundaries. Nanoparticles were collected on polished Si wafers placed beneath the discharge during operation, and complementary analyses were performed on the electrodes before and after long-term plasma exposure (Fig. 6A). Full experimental details provided in the SI Section 1.4. In this pin-to-pin configuration, the pointed electrode served as the cathode and the flat electrode as the anode, a fixed polarity determined by the nanosecond pulsed power supply. Both electrodes showed evidence of plasma-induced modification, though to different extents: the pointed cathode tip exhibited pronounced erosion and localized melting (Fig. S5F), consistent with the concentrated electric field at the tip and intense ion bombardment from the cathode fall, while the flat anode showed microcrater formation and nanoparticle generation under comparatively milder conditions (Fig. 6C).

The flat anode surface shows clear evidence of erosion and chemical modification after extended operation, while the pointed cathode tip exhibits pronounced erosion (SI Fig. S5E and F). Before plasma exposure, wide-field SEM images show a clean metallic surface. However, after 54×10^6 pulses, the same region has pits, roughening, and redeposited material (Fig. 6C). The orange box highlights the spark attachment zone, the region where the discharge repeatedly contacts the electrode, which shows the most pronounced morphological changes, appearing as bright, textured features consistent with localized heating and material redistribution. The light regions within this zone correspond to micro-melt pools formed by localized arc attachment, exhibiting smooth, resolidified surfaces surrounded by ejected debris (Fig. S5D). A higher-magnification view of this spark attachment zone (blue box) reveals surface texturing from repeated discharge events. At the electrode edge (green box), away from the primary spark attachment zone, nanoparticles accumulate through redeposition of material

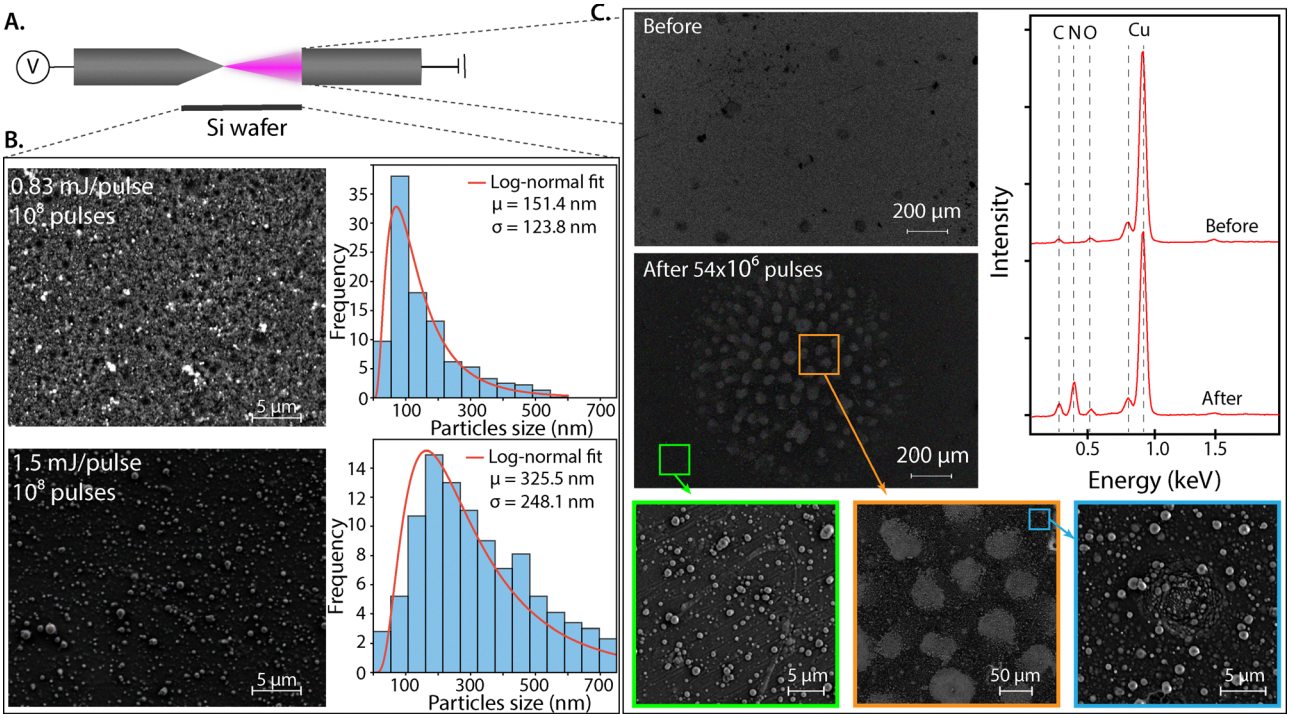

Fig. 6 SEM-EDX of plasma-generated nanoparticles on Si and electrode surface changes. (A) Schematic of sampling configuration: nanoparticles were collected on polished Si wafers beneath the discharge, while electrode surfaces were examined before and after plasma operation. (B) SEM images and corresponding size distributions of nanoparticles collected on Si wafers under identical $N_2:H_2 = 1:3$ feed (4 sccm total flow) with the same number of pulses. Top: 0.83 mJ pulse^{-1}; bottom: 1.5 mJ pulse^{-1}. At higher energy, both particle density and size increase, with distributions broadening toward larger diameters. (C) SEM of the Cu electrode before and after 54 × 10^6 pulses: the spark-active region (orange) and its zoom (blue) reveal filament-induced cratering, while the edge (green) shows redeposited particles. EDX spectra confirm nitrogen incorporation after plasma exposure.

transported from the discharge-active region. This spatial distribution, intense modification at the spark zone and particle accumulation at peripheral regions, is consistent with electrode erosion and redeposition mechanisms in pulsed spark discharges. EDX spectra acquired from the same electrode surface region before and after plasma exposure support this interpretation: the post-plasma spectrum shows nitrogen peaks at 0.39 keV, indicating surface nitridation. The minor increase in carbon signal observed in post-plasma spectra is attributed to adventitious carbon contamination during sample transfer between the reactor and SEM chamber, a common artifact for air-exposed surfaces.

Under the same gas feed ($N_2:H_2 = 1:3$, 4 sccm total flow rate) and same number of pulses (~10^8 pulses), the particle population changed strongly with the discharge energy (Fig. 6B). At ~0.83 mJ pulse^{-1}, only a thin layer of relatively small particles was collected, with a log-normal size distribution centered at μ = 151.4 nm (σ = 123.8 nm). Most particles stayed below 300 nm, giving a fairly narrow distribution. When the energy was increased to ~1.5 mJ pulse^{-1}, the surface was instead covered with a dense layer of near spherical particles, and the histogram shifted to much larger sizes with μ = 325.5 nm (σ = 248.1 nm), extending out toward 700 nm. Because of the increased particle number and size, higher energy sparks inject more catalytically active material into the discharge, extending the accessible surface area and possibly introducing new active phases. Control experiments with doubled exposure time (~2 × 10^8 pulses) at 0.83 mJ pulse^{-1} yield a similar size distribution (Fig. S5C), confirmed that particle size is governed primarily by instantaneous pulse energy rather than total accumulated energy, indicating that ablation dynamics during individual discharge events control nanoparticle formation. As a result, pulse energy not only governs electrode erosion but also alters the nanoparticle population that participates in plasma-driven chemistry.

These findings suggest that nanoparticles are continuously produced from the electrodes during plasma operation. Pulse energy acts as a direct control over their yield and size, while long-term runs reshape and chemically age the electrodes themselves. In practice, this means that even in systems described as "catalyst-free," the electrodes act as a built-in source of catalytic nanoparticles.

5.4 Compositional changes of electrodes

Nanoparticles were collected on polished Si wafers beneath the discharge, using the same sample configuration as in Fig. 6A. Each sample was exposed to 10^8 pulses at 0.83 mJ pulse^{-1}, under either $N_2:H_2 = 1:3$ or 1:7 feeds. After collecting, Si substrates were examined using X-ray photoelectron spectroscopy (XPS) (details in SI S1.4). XPS shows that the chemical state of Cu nanoparticles released from the electrodes depends strongly on the N_2/H_2 ratio (Fig. 7). In the Cu $2p_{3/2}$ region, metallic Cu^0 appears at 932.6 eV with overlapping Cu^+ features

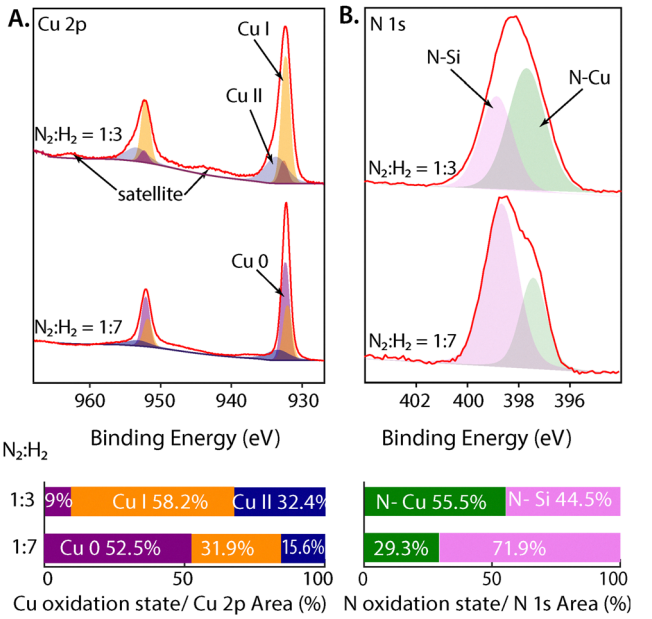

Fig. 7 XPS of particles collected on Si wafer after 10^8 pulses at 0.83 mJ pulse^{-1} under $N_2:H_2 = 1:3$ or 1:7. (A) Cu 2p with fitted Cu^0, Cu^+, Cu^{2+} states. (B) N 1s with N–Cu and N–Si signals. Bar plots show relative fractions.

at 932.7 eV, while a weaker signal at 933.8 eV, characteristic of Cu^{2+}, is observed; because the plasma reactor was oxygen-free, this Cu^{2+} contribution is attributed to atmospheric contamination during sample transport to the XPS chamber rather than in-plasma chemistry.[109–111] Quantification from Cu LMM Auger spectra (SI Section 5) reveals that under N_2-rich feed ($N_2:H_2$ = 1:3), the nanoparticles were dominated by Cu^+(58.2%) with smaller fractions of Cu^{2+} (32.4%) and Cu^0 (9.0%).[112] Nitrogen bound to Cu accounted for 55.5% of the total N signal,[110,111,113] while the remainder (44.5%) was assigned to N adsorbed on the Si substrate. In contrast, under H_2-rich feed ($N_2:H_2$ = 1:7), metallic Cu^0 increased to 52.5% with Cu^+ at 31.9% and Cu^{2+} reduced to 15.6%. Here, the Cu–N fraction dropped to 29.3%, while Si–N adsorption dominated at 71.9%. The N 1s spectra corroborates these results: a distinct peak at ~397.8 eV, characteristic of Cu–N bonding, is prominent in the N_2-rich case but strongly suppressed under H_2-rich conditions. This quantitative comparison confirms that hydrogen-rich conditions suppress surface nitridation, excess hydrogen increases the probability that activated nitrogen is hydrogenated to NH_3 rather than stored as Cu–N phases.

Despite the stronger nitridation signature at 1:3 feed, the 1:7 feed produced the higher NH_3 yield. This contrast can be rationalized by stoichiometric considerations and competing reaction pathways. The H_2-rich mixture supplies over twice the stoichiometric hydrogen, raising the chance that each activated N atom is fully hydrogenated rather than stored as a nitride. In this regime, hydrogenation becomes probability-driven: abundant H_2 and H radicals shift the chemistry toward NH_3 release instead of lattice storage. Quantitatively, the 1:7 condition (87.5% H_2) increased NH_3 yield about sevenfold – from 0.3% to 2.2% – even at constant SEI, while the N_2/H_2 conversion ratio fell from 5–5.7 (at 1:3) to 0.8–1.2 (at 1:7), showing that nitrogen was no longer trapped in the electrode. The XPS confirms this trend: Cu–N accounted for ~55% of the total N signal at 1:3 but only ~29% at 1:7, meaning less nitrogen was locked as Cu_3N-like phases. Together, these results indicate that excess hydrogen suppresses nitride formation and maintains more metallic surface sites for catalysis. Concurrently, spark erosion continuously delivers Cu/Cu–N nanoparticles that coat internal surfaces, extending the effective catalytic area beyond the geometric electrode boundary. Overall, the XPS and performance data together reveal dynamic electrode-supplied catalysis: while both feed ratios activate nitrogen through the electrode, hydrogen-rich conditions minimize unproductive nitrogen storage in nitrides and maximize NH_3 production, whereas nitrogen-rich conditions favor nitride formation that acts as a nitrogen sink.

The coexistence of metallic Cu and Cu–N phases has important catalytic implications for the design and optimization of plasma processes. Copper nitride has different electronic structure than metallic Cu, with modified d-band characteristics that alter nitrogen adsorption energies and hydrogenation barriers. The active surface during plasma operation is therefore not pure metal but a dynamic mixture of phases, and the observed catalytic behavior reflects this mixed-phase composition. The correlation between feed ratio, surface nitridation, and NH_3 yield suggests that maintaining metallic Cu sites is beneficial for ammonia production: hydrogen-rich conditions suppress nitride formation, preserve metallic surface character, and produce sevenfold higher NH_3 yields. This phase-dependent behavior extends to electrode material selection, W forms highly stable nitrides that could lock nitrogen in inactive phases, contributing to W's poor performance, whereas the less stable copper nitride allows more dynamic nitrogen exchange between surface and gas phase.[113]

6. Are electrode plasmas ever catalyst-free?

Plasma systems with metal electrodes in direct contact with discharges exhibit catalytic reactions in addition to the volumetric plasma-phase chemistry that has traditionally been emphasized. The combined evidence from literature and our experiments demonstrates that electrodes catalyze plasma reactions actively by both driving surface reactions and the production of nanoparticle impurities that coat surfaces, rather than merely emitting electrons to sustain discharges. As outlined in Section 4, electrode composition and morphology have been shown to alter plasma chemistry across different discharge types and energy conditions within plasmas even in the absence of packed beds. Early glow discharge studies showed that changing only the electrode metal shifted NH_3 production rates, while later work with wool-like pads or tangled-wire electrodes achieved large improvements in yield and energy efficiency. Comparable activity has been observed across CO_2, CH_4, and NH_3 systems, confirming electrode catalysis as a universal

phenomenon. In our spark discharge case study, this effect becomes quantifiable: under identical discharge settings, Ni electrodes produced 0.37% NH_3 yield, Cu 0.32%, SS 304 0.23%, and W only 0.11%, variations far beyond experimental uncertainty. Most dramatically, changing the feed from $N_2:H_2 = 1:3$ to 1 : 7 on Cu electrodes increased NH_3 yield sevenfold to 2.2%. Surface analyses revealed the underlying mechanisms: nitridation creates dynamic nitrogen reservoirs, erosion generates catalytic nanoparticles, and redeposition spreads these particles throughout the reactor.

These catalytic effects arise because plasma conditions couple directly to electrodes as boundary conditions. While electrodes act as emissive elements to sustain discharges, ion bombardment and localized heating also drive surface reactions that evolve dynamically during operation. Continuous ion bombardment refreshes active sites, sputtering exposes fresh metal, and strong electric fields enhance surface reactivity. Even refractory metals erode under plasma exposure, releasing nanoparticles that seed new catalytic sites across the reactor. As a result, electrodes cannot be treated as passive current carriers, they act as chemically active participants whose composition and morphology shape the performance of plasma chemical processes. Recognizing this opens opportunities: rather than choosing electrodes solely for conductivity or durability, they can be deliberately engineered as catalytic elements. In turn, more accurate and reproducible plasma chemical mechanisms, including where products form and how intermediates couple, can be achieved.

Opportunities to tailor plasma reactions expand dramatically when electrodes are treated as catalytic elements rather than passive conductors. Alloying electrode materials can optimize catalytic properties by tuning the d-band center and modifying binding energies of key intermediates. Protective coatings offer another lever, offering a mechanism to maintain catalytically active phases while mitigating erosion and limiting redeposition of sputtered material onto other reactor surfaces. Electrode geometry provides yet another design dimension: wool-like pads or tangled-wire meshes introduce large surface areas and diverse active sites, sustaining high ion fluxes and enhancing radical-surface coupling. By engineering the surface geometry and chemistry of electrodes, there are opportunities to promote favorable surface-assisted pathways to enhance both the selectivity and energy efficiency of processes directly. Importantly, plasma continuously refreshes electrode surfaces, *via* ion bombardment, sputtering, and redeposition, so active sites are regenerated rather than deactivated. This self-renewing feature gives plasma-catalyst electrodes a distinct advantage over conventional heterogeneous catalysts, which are often susceptible to poisoning or sintering depending on the kinetics and mechanisms of particular chemical processes.

To fully realize these opportunities, the field must broaden mechanistic investigations of plasma processes to include the surface chemistry occurring at electrode interfaces explicitly. Stainless steel is a common electrode material in plasma reactors and is often assumed to be ''inert.'' Our results show that SS 304 contributes catalytically measurably to ammonia synthesis, falling between Cu and W in performance. Studies should therefore document electrode design and geometry, including material composition and purity, surface preparation methods, operational changes during use (such as color shifts, roughening, or mass loss), and post-reaction characterization, to ensure reproducibility. Models and mechanistic frameworks must account for the catalytic roles of electrodes, as well as their potential to introduce impurities into other phases and interfaces through erosion and redeposition. In this context, terms like ''catalyst-free'' become difficult to justify without clear mechanistic evidence that electrodes contribute negligibly to the observed chemistry. Without these changes in practice and terminology, electrode effects will remain hidden variables in plasma systems, obscuring mechanisms, compromising reproducibility, and hindering their optimization.''

7. Conclusions

This study demonstrates that plasma chemical processes are rarely ''catalyst-free.'' Even in the absence of dispersed heterogeneous catalysts, surfaces that bound the plasma – such as electrodes-act as chemically active sites where catalytic reactions occur. These surfaces influence the local plasma environment, undergo erosion and composition changes, and continuously supply nanoparticles into the discharge. Far from incidental, these processes directly affect yields, selectivity, and mechanistic pathways.

We propose a classification framework that makes electrode contributions visible from the outset, linking plasma catalytic behavior to the nature of both external and internal boundaries. Combining literature analysis with our spark-discharge case study, we show that electrode material, surface chemistry, and nanoparticle generation all leave measurable imprints on plasma reactions. Systems long considered ''catalyst-free'' in fact experience catalytic effects from electrodes, either through surface reactions or by injecting nanoparticles into other phases. Recognizing electrodes as catalytic elements is therefore essential for accurate mechanistic understanding and benchmarking of plasma processes. Reporting electrode composition, surface condition, and signs of particle generation should become standard practice. Looking forward, treating electrodes as tunable catalytic elements rather than passive current carriers opens the door to systematic design strategies where electrode engineering can be directly linked to plasma chemistry and reaction mechanisms.

Author contributions

Conceptualization: T. C. U., T. V. L., C. B. M. Methodology: T. V. L., T. C. U., C. B. M. Investigation: T. V. L. Data curation: T. V. L. Formal analysis: T. V. L., T. C. U. Visualization: T. V. L. Writing – original draft: T. V. L. Writing – review & editing: T. C. U., T. V. L., C. B. M. Supervision: C. B. M., T. C. U.

Conflicts of interest

There are no conflicts to declare.

Data availability

Additional raw datasets are available from the author on reasonable request.

All data supporting this study are provided in the main text and supplementary information (SI). Supplementary information is available. See DOI: https://doi.org/10.1039/d5ey00305a.

Acknowledgements

This work was supported by the National Science Foundation under Award Number 2453911, through the ECosystem for Leading Innovation in Plasma Science and Engineering (ECLIPSE) program. The authors also acknowledge the support of the seed grant program through the Energy Institute at The University of Texas at Austin.

References

1 J. C. Whitehead, Plasma–catalysis: the known knowns, the known unknowns and the unknown unknowns, *J. Phys. D: Appl. Phys.*, 2016, **49**, 243001.
2 A. Bogaerts, X. Tu, J. C. Whitehead, G. Centi, L. Lefferts, O. Guaitella, F. Azzolina-Jury, H.-H. Kim, A. B. Murphy, W. F. Schneider, T. Nozaki, J. C. Hicks, A. Rousseau, F. Thevenet, A. Khacef and M. Carreon, The 2020 plasma catalysis roadmap, *J. Phys. D: Appl. Phys.*, 2020, **53**, 443001.
3 M. L. Carreon, Plasma catalysis: a brief tutorial, *Plasma Res. Express*, 2019, **1**, 043001.
4 P. Mehta, P. Barboun, D. B. Go, J. C. Hicks and W. F. Schneider, Catalysis Enabled by Plasma Activation of Strong Chemical Bonds: A Review, *ACS Energy Lett.*, 2019, **4**, 1115–1133.
5 P. Mehta, P. Barboun, F. A. Herrera, J. Kim, P. Rumbach, D. B. Go, J. C. Hicks and W. F. Schneider, Overcoming ammonia synthesis scaling relations with plasma-enabled catalysis, *Nat. Catal.*, 2018, **1**, 269–275.
6 M. Iwamoto, M. Akiyama, K. Aihara and T. Deguchi, Ammonia Synthesis on Wool-Like Au, Pt, Pd, Ag, or Cu Electrode Catalysts in Nonthermal Atmospheric-Pressure Plasma of N_2 and H_2, *ACS Catal.*, 2017, **7**, 6924–6929.
7 Y. Wang, M. Craven, X. Yu, J. Ding, P. Bryant, J. Huang and X. Tu, Plasma-Enhanced Catalytic Synthesis of Ammonia over a Ni/Al_2O_3 Catalyst at Near-Room Temperature: Insights into the Importance of the Catalyst Surface on the Reaction Mechanism, *ACS Catal.*, 2019, **9**, 10780–10793.
8 K. H. R. Rouwenhorst, H. G. B. Burbach, D. W. Vogel, J. Núñez Paulí, B. Geerdink and L. Lefferts, Plasma-catalytic ammonia synthesis beyond thermal equilibrium on Ru-based catalysts in non-thermal plasma, *Catal. Sci. Technol.*, 2021, **11**, 2834–2843.
9 H. Kim, Y. Teramoto, A. Ogata, H. Takagi and T. Nanba, Atmospheric–pressure nonthermal plasma synthesis of ammonia over ruthenium catalysts, *Plasma Processes Polym.*, 2017, **14**, 1600157.
10 R. Snoeckx and A. Bogaerts, Plasma technology – a novel solution for CO_2 conversion?, *Chem. Soc. Rev.*, 2017, **46**, 5805–5863.
11 S. Liu, L. R. Winter and J. G. Chen, Review of Plasma-Assisted Catalysis for Selective Generation of Oxygenates from CO_2 and CH_4, *ACS Catal.*, 2020, **10**, 2855–2871.
12 C. R. Nallapareddy and T. C. Underwood, Tailoring Vibrational Excitation Pathways for High-Yield Oxidation of Methane to Methanol, *ACS Sustainable Chem. Eng.*, 2024, **12**, 9144–9155.
13 N. Wang, H. O. Otor, G. Rivera-Castro and J. C. Hicks, Plasma Catalysis for Hydrogen Production: A Bright Future for Decarbonization, *ACS Catal.*, 2024, **14**, 6749–6798.
14 H. L. Chen, H. M. Lee, S. H. Chen, M. B. Chang, S. J. Yu and S. N. Li, Removal of Volatile Organic Compounds by Single-Stage and Two-Stage Plasma Catalysis Systems: A Review of the Performance Enhancement Mechanisms, Current Status, and Suitable Applications, *Environ. Sci. Technol.*, 2009, **43**, 2216–2227.
15 Z. D. Feng, A. King, J. Diao, C. Leung, H. Kim, H. Park, G. Henkelman, C. B. Mullins and T. C. Underwood, Mitigating Surface Deactivation for N_2 O Abatement Using Plasma Activated Co-reactants, *ACS Catal.*, 2025, **15**, 13970–13984.
16 K. Ouaras, G. Lombardi and K. Hassouni, Nanoparticles synthesis in microwave plasmas: peculiarities and comprehensive insight, *Sci. Rep.*, 2024, **14**, 4653.
17 X. Lu, P. J. Bruggeman, S. Reuter, G. Naidis, A. Bogaerts, M. Laroussi, M. Keidar, E. Robert, J.-M. Pouvesle, D. Liu and K. (Ken) Ostrikov, Grand challenges in low temperature plasmas, *Front. Phys.*, 2022, **10**, 1040658.
18 M. A. Lieberman and A. J. Lichtenberg, *Principles of Plasma Discharges and Materials Processing*, Wiley, 1st edn, 2005.
19 H. Kim, Y. Teramoto, A. Ogata, H. Takagi and T. Nanba, Atmospheric–pressure nonthermal plasma synthesis of ammonia over ruthenium catalysts, *Plasma Processes Polym.*, 2017, **14**, 1600157.
20 L. R. Winter, B. Ashford, J. Hong, A. B. Murphy and J. G. Chen, Identifying Surface Reaction Intermediates in Plasma Catalytic Ammonia Synthesis, *ACS Catal.*, 2020, **10**, 14763–14774.
21 E. C. Neyts, K. (Ken) Ostrikov, M. K. Sunkara and A. Bogaerts, Plasma Catalysis: Synergistic Effects at the Nanoscale, *Chem. Rev.*, 2015, **115**, 13408–13446.
22 V. Rosa, F. Cameli, G. D. Stefanidis and K. M. Van Geem, Integrating Materials in Non-Thermal Plasma Reactors: Challenges and Opportunities, *Acc. Mater. Res.*, 2024, **5**, 1024–1035.
23 E. C. Neyts and A. Bogaerts, Understanding plasma catalysis through modelling and simulation—a review, *J. Phys. D: Appl. Phys.*, 2014, **47**, 224010.
24 K. Van Laer and A. Bogaerts, Influence of Gap Size and Dielectric Constant of the Packing Material on the Plasma Behaviour in a Packed Bed DBD Reactor: A Fluid Modelling Study, *Plasma Processes Polym.*, 2017, **14**, 1600129.
25 Y.-R. Zhang, E. C. Neyts and A. Bogaerts, Influence of the Material Dielectric Constant on Plasma Generation inside Catalyst Pores, *J. Phys. Chem. C*, 2016, **120**, 25923–25934.

26 E. Slikboer, K. Acharya, A. Sobota, E. Garcia-Caurel and O. Guaitella, Revealing Plasma-Surface Interaction at Atmospheric Pressure: Imaging of Electric Field and Temperature inside the Targeted Material, *Sci. Rep.*, 2020, **10**, 2712.
27 I. Belov, S. Paulussen and A. Bogaerts, Appearance of a conductive carbonaceous coating in a CO_2 dielectric barrier discharge and its influence on the electrical properties and the conversion efficiency, *Plasma Sources Sci. Technol.*, 2016, **25**, 015023.
28 L. L. Alves, M. M. Becker, J. Van Dijk, T. Gans, D. B. Go, K. Stapelmann, J. Tennyson, M. M. Turner and M. J. Kushner, Foundations of plasma standards, *Plasma Sources Sci. Technol.*, 2023, **32**, 023001.
29 K. S. Yin and M. Venugopalan, Plasma chemical synthesis. I. Effect of electrode material on the synthesis of ammonia, *Plasma Chem. Plasma Process.*, 1983, **3**, 343–350.
30 Y. Ma, Y. Tian, Y. Zeng and X. Tu, Plasma synthesis of ammonia in a tangled wire dielectric barrier discharge reactor: Effect of electrode materials, *J. Energy Inst.*, 2021, **99**, 137–144.
31 R. De Meyer, J. Verbeeck, S. Bals and A. Bogaerts, Contamination in Dielectric Barrier Discharge Plasmas by Electrode Erosion, *ACS Mater. Lett.*, 2025, **7**, 52–58.
32 L. Jiang, Q. Li, D. Zhu, M. Attoui, Z. Deng, J. Tang and J. Jiang, Comparison of nanoparticle generation by two plasma techniques: Dielectric barrier discharge and spark discharge, *Aerosol Sci. Technol.*, 2017, **51**, 206–213.
33 W. Ye, J. Cao, J. Wang and H. Wu, Advancements in Metallic Electrode Materials for Plasma Discharges Applications: Corrosion and Erosion Mechanisms in Liquid Phase Discharges, *Plasma Chem. Plasma Process.*, 2025, **45**, 1313–1336.
34 U. R. Kortshagen, R. M. Sankaran, R. N. Pereira, S. L. Girshick, J. J. Wu and E. S. Aydil, Nonthermal Plasma Synthesis of Nanocrystals: Fundamental Principles, Materials, and Applications, *Chem. Rev.*, 2016, **116**, 11061–11127.
35 S. L. Girshick, Particle nucleation and growth in dusty plasmas: On the importance of charged-neutral interactions, *J. Vac. Sci. Technol., A*, 2020, **38**, 011001.
36 V. S. Subhankar, C. R. Nallapareddy, C. B. Mullins and T. C. Underwood, Plasma-Enabled Catalytic Design to Upgrade Methane Directly and Limit Coking, *ACS Catal.*, 2025, **15**, 10433–10447.
37 V. S. Subhankar, C. R. Nallapareddy and T. C. Underwood, *AIAA SCITECH 2024 Forum*, American Institute of Aeronautics and Astronautics, Orlando, FL, 2024.
38 V. S. Subhankar, A. Saha, S. Gershman and T. C. Underwood, Decoupling plasma, catalyst, and gaseous mechanisms for non-oxidative methane conversion, *Plasma Sources Sci. Technol.*, 2026, DOI: 10.1088/1361-6595/ae477a.
39 R. I. Masel, *Principles of adsorption and reaction on solid surfaces*, Wiley, New York, NY, 1996.
40 S. Kumar, H. Jiang, M. Schwarzer, A. Kandratsenka, D. Schwarzer and A. M. Wodtke, Vibrational Relaxation Lifetime of a Physisorbed Molecule at a Metal Surface, *Phys. Rev. Lett.*, 2019, **123**, 156101.
41 V. Krishna and J. C. Tully, Vibrational lifetimes of molecular adsorbates on metal surfaces, *J. Chem. Phys.*, 2006, **125**, 054706.
42 J. Shah, W. Wang, A. Bogaerts and M. L. Carreon, Ammonia Synthesis by Radio Frequency Plasma Catalysis: Revealing the Underlying Mechanisms, *ACS Appl. Energy Mater.*, 2018, **1**, 4824–4839.
43 V. S. Subhankar, J. Diao, C. C. Leung, Z. D. Feng, S. Gershman, J. Steele, M. Baldea, G. Henkelman, C. B. Mullins and T. C. Underwood, Plasma-Enabled Active Site Regeneration for Selective Liquid Fuel Production across Catalyst Binding Regimes in CH_4–CO_2 Conversion, *Chemistry*, 2025, DOI: 10.26434/chemrxiv-2025-5vvh3.
44 M.-Y. Song, J.-S. Yoon, H. Cho, Y. Itikawa, G. P. Karwasz, V. Kokoouline, Y. Nakamura and J. Tennyson, Cross Sections for Electron Collisions with Methane, *J. Phys. Chem. Ref. Data*, 2015, **44**, 023101.
45 M. Daksha, A. Derzsi, S. Wilczek, J. Trieschmann, T. Mussenbrock, P. Awakowicz, Z. Donkó and J. Schulze, The effect of realistic heavy particle induced secondary electron emission coefficients on the electron power absorption dynamics in single- and dual-frequency capacitively coupled plasmas, *Plasma Sources Sci. Technol.*, 2017, **26**, 085006.
46 L. Wang, P. Hartmann, Z. Donkó, Y.-H. Song and J. Schulze, 2D particle-in-cell simulations of geometrically asymmetric low-pressure capacitive RF plasmas driven by tailored voltage waveforms, *Plasma Sources Sci. Technol.*, 2021, **30**, 054001.
47 D. Pye, *Practical Nitriding and Ferritic Nitrocarburizing*, ASM International, 2003.
48 N. Benard and E. Moreau, Electrical and mechanical characteristics of surface AC dielectric barrier discharge plasma actuators applied to airflow control, *Exp. Fluids*, 2014, **55**, 1846.
49 Y. Gao, L. Dou, B. Feng, C. Zhang and T. Shao, Catalyst-free activation of CH_4 and air into platform chemicals and H_2 using parametrized nanosecond pulsed plasma, *Energy Convers. Manage.*, 2023, **276**, 116570.
50 T. Zhang, J. Knezevic, M. Zhu, J. Hong, R. Zhou, Q. Song, L. Ding, J. Sun, D. Liu, K. K. Ostrikov, R. Zhou and P. J. Cullen, Catalyst-Free Carbon Dioxide Conversion in Water Facilitated by Pulse Discharges, *J. Am. Chem. Soc.*, 2023, **145**, 28233–28239.
51 F. Chu, G. Zhao, W. Li, W. Wei, W. Chen, Z. Ma, Z. Gao, N. S. Shuaibu, J. Luo, B. Yu, H. Feng, Y. Pan and X. Wang, Catalyst-Free Oxidation Reactions in a Microwave Plasma Torch-Based Ion/Molecular Reactor: An Approach for Predicting the Atmospheric Oxidation of Pollutants, *Anal. Chem.*, 2023, **95**, 2004–2010.
52 Y. Wang, Y. Chen, J. Harding, H. He, A. Bogaerts and X. Tu, Catalyst-free single-step plasma reforming of CH_4 and CO_2 to higher value oxygenates under ambient conditions, *Chem. Eng. J.*, 2022, **450**, 137860.
53 R. Hawtof, S. Ghosh, E. Guarr, C. Xu, R. Mohan Sankaran and J. N. Renner, Catalyst-free, highly selective synthesis of ammonia from nitrogen and water by a plasma electrolytic system, *Sci. Adv.*, 2019, **5**, eaat5778.

54 X. Zhang, R. Su, J. Li, L. Huang, W. Yang, K. Chingin, R. Balabin, J. Wang, X. Zhang, W. Zhu, K. Huang, S. Feng and H. Chen, Efficient catalyst-free N2 fixation by water radical cations under ambient conditions, *Nat. Commun.*, 2024, **15**, 1535.
55 B. Huang, C. Zhang, H. Bai, S. Zhang, K. (Ken) Ostrikov and T. Shao, Energy pooling mechanism for catalyst-free methane activation in nanosecond pulsed non-thermal plasmas, *Chem. Eng. J.*, 2020, **396**, 125185.
56 H. Hu, N. Liu, Q. Ru, W. Jiang, Y. Yang, K. Ma, L. Meng, Z. Du, B. Zhang and G. Cheng, Highly selective, catalyst-free CO_2 reduction in strong acid without alkali cations by a mechanical energy-induced triboelectric plasma-electrolytic system, *Green Chem.*, 2025, **27**, 6747–6753.
57 R. Zhou, R. Zhou, Y. Xian, Z. Fang, X. Lu, K. Bazaka, A. Bogaerts and K. (Ken), Ostrikov, Plasma-enabled catalyst-free conversion of ethanol to hydrogen gas and carbon dots near room temperature, *Chem. Eng. J.*, 2020, **382**, 122745.
58 K. Van Laer and A. Bogaerts, Fluid modelling of a packed bed dielectric barrier discharge plasma reactor, *Plasma Sources Sci. Technol.*, 2016, **25**, 015002.
59 D. Z. Pai, D. A. Lacoste and C. O. Laux, Nanosecond repetitively pulsed discharges in air at atmospheric pressure—the spark regime, *Plasma Sources Sci. Technol.*, 2010, **19**, 065015.
60 S. Kolev and A. Bogaerts, A 2D model for a gliding arc discharge, *Plasma Sources Sci. Technol.*, 2014, **24**, 015025.
61 X. Tu and J. C. Whitehead, Plasma-catalytic dry reforming of methane in an atmospheric dielectric barrier discharge: Understanding the synergistic effect at low temperature, *Appl. Catal., B*, 2012, **125**, 439–448.
62 D. Mei, P. Zhang, G. Duan, S. Liu, Y. Zhou, Z. Fang and X. Tu, CH_4 reforming with CO_2 using a nanosecond pulsed dielectric barrier discharge plasma, *J. CO2 Util.*, 2022, **62**, 102073.
63 W. Wang, H.-H. Kim, K. Van Laer and A. Bogaerts, Streamer propagation in a packed bed plasma reactor for plasma catalysis applications, *Chem. Eng. J.*, 2018, **334**, 2467–2479.
64 Y. Gorbanev, E. Vervloessem, A. Nikiforov and A. Bogaerts, Nitrogen Fixation with Water Vapor by Nonequilibrium Plasma: toward Sustainable Ammonia Production, *ACS Sustainable Chem. Eng.*, 2020, **8**, 2996–3004.
65 A. Fridman, A. Chirokov and A. Gutsol, Non-thermal atmospheric pressure discharges, *J. Phys. D: Appl. Phys.*, 2005, **38**, R1–R24.
66 K. V. Karthikeyan and R. Harish, Advancements in flow control using plasma actuators: a comprehensive review, *Eng. Res. Express*, 2025, **7**, 012502.
67 Y. Ren, C. Yu, L. Wang, X. Tan, Z. Wang, Q. Wei, Y. Zhang and J. Qiu, Microscopic-Level Insights into the Mechanism of Enhanced NH_3 Synthesis in Plasma-Enabled Cascade N_2 Oxidation–Electroreduction System, *J. Am. Chem. Soc.*, 2022, **144**, 10193–10200.
68 S. K. Sengupta and O. P. Singh, Contact glow discharge electrolysis: a study of its chemical yields in aqueous inert-type electrolytes, *J. Electroanal. Chem.*, 1994, **369**, 113–120.
69 J. A. Andersen, J. M. Christensen, M. Østberg, A. Bogaerts and A. D. Jensen, Plasma-catalytic dry reforming of methane: Screening of catalytic materials in a coaxial packed-bed DBD reactor, *Chem. Eng. J.*, 2020, **397**, 125519.
70 D. Mei, M. Sun, S. Liu, P. Zhang, Z. Fang and X. Tu, Plasma-enabled catalytic dry reforming of CH4 into syngas, hydrocarbons and oxygenates: Insight into the active metals of γ-Al_2O_3 supported catalysts, *J. CO2 Util.*, 2023, **67**, 102307.
71 M. Q. Feliz, I. Polaert, A. Ledoux, C. Fernandez and F. Azzolina-Jury, Influence of ionic conductivity and dielectric constant of the catalyst on DBD plasma-assisted CO_2 hydrogenation into methanol, *J. Phys. D: Appl. Phys.*, 2021, **54**, 334003.
72 B. Eliasson, U. Kogelschatz, B. Xue and L.-M. Zhou, Hydrogenation of Carbon Dioxide to Methanol with a Discharge-Activated Catalyst, *Ind. Eng. Chem. Res.*, 1998, **37**, 3350–3357.
73 X. Yang, C. Richards and I. V. Adamovich, Ammonia generation in Ns pulse and Ns pulse/RF discharges over a catalytic surface, *Plasma Sources Sci. Technol.*, 2023, **32**, 064003.
74 K. Aihara, M. Akiyama, T. Deguchi, M. Tanaka, R. Hagiwara and M. Iwamoto, Remarkable catalysis of a wool-like copper electrode for NH_3 synthesis from N_2 and H_2 in non-thermal atmospheric plasma, *Chem. Commun.*, 2016, **52**, 13560–13563.
75 C. Wildfire, V. Abdelsayed, D. Shekhawat and M. J. Spencer, Ambient pressure synthesis of ammonia using a microwave reactor, *Catal. Commun.*, 2018, **115**, 64–67.
76 X. Zhu, X. Hu, X. Wu, Y. Cai, H. Zhang and X. Tu, Ammonia synthesis over γ-Al_2O_3 pellets in a packed-bed dielectric barrier discharge reactor, *J. Phys. D: Appl. Phys.*, 2020, **53**, 164002.
77 P. Barboun, P. Mehta, F. A. Herrera, D. B. Go, W. F. Schneider and J. C. Hicks, Distinguishing Plasma Contributions to Catalyst Performance in Plasma-Assisted Ammonia Synthesis, *ACS Sustainable Chem. Eng.*, 2019, **7**, 8621–8630.
78 A. Gómez-Ramírez, J. Cotrino, R. M. Lambert and A. R. González-Elipe, Efficient synthesis of ammonia from N_2 and H_2 alone in a ferroelectric packed-bed DBD reactor, *Plasma Sources Sci. Technol.*, 2015, **24**, 065011.
79 S. Li, T. Van Raak and F. Gallucci, Investigating the operation parameters for ammonia synthesis in dielectric barrier discharge reactors, *J. Phys. D: Appl. Phys.*, 2020, **53**, 014008.
80 J. Shah, T. Wu, J. Lucero, M. A. Carreon and M. L. Carreon, Nonthermal Plasma Synthesis of Ammonia over Ni-MOF-74, *ACS Sustainable Chem. Eng.*, 2019, **7**, 377–383.
81 J. Hong, M. Aramesh, O. Shimoni, D. H. Seo, S. Yick, A. Greig, C. Charles, S. Prawer and A. B. Murphy, Plasma Catalytic Synthesis of Ammonia Using Functionalized-Carbon Coatings in an Atmospheric-Pressure Non-equilibrium Discharge, *Plasma Chem. Plasma Process.*, 2016, **36**, 917–940.
82 G. Zhou, H. Zhao, X. Wang, Z. Wang, Y. Zhang, X. Zhao, Q. Chen, T. Chen, Z. Huang and H. Lin, Plasma-catalytic

ammonia synthesis on Ni catalysts supported on Al_2O_3, Si-MCM-41 and SiO_2, *Int. J. Hydrogen Energy*, 2024, **60**, 802–813.

83 X. Hu, X. Zhu, X. Wu, Y. Cai and X. Tu, Plasma-enhanced NH_3 synthesis over activated carbon-based catalysts: effect of active metal phase, *Plasma Processes Polym.*, 2020, **17**, 2000072.

84 G. Akay and K. Zhang, Process Intensification in Ammonia Synthesis Using Novel Coassembled Supported Microporous Catalysts Promoted by Nonthermal Plasma, *Ind. Eng. Chem. Res.*, 2017, **56**, 457–468.

85 Y. Wang, W. Yang, S. Xu, S. Zhao, G. Chen, A. Weidenkaff, C. Hardacre, X. Fan, J. Huang and X. Tu, Shielding Protection by Mesoporous Catalysts for Improving Plasma-Catalytic Ambient Ammonia Synthesis, *J. Am. Chem. Soc.*, 2022, **144**, 12020–12031.

86 J. Nakajima and H. Sekiguchi, Synthesis of ammonia using microwave discharge at atmospheric pressure, *Thin Solid Films*, 2008, **516**, 4446–4451.

87 R. Aerts, W. Somers and A. Bogaerts, Carbon Dioxide Splitting in a Dielectric Barrier Discharge Plasma: A Combined Experimental and Computational Study, *ChemSusChem*, 2015, **8**, 702–716.

88 M. S. Bak, S.-K. Im and M. Cappelli, Nanosecond-pulsed discharge plasma splitting of carbon dioxide, *IEEE Trans. Plasma Sci.*, 2015, **43**, 1002–1007.

89 A. Bogaerts, T. Kozák, K. Van Laer and R. Snoeckx, Plasma-based conversion of CO_2: current status and future challenges, *Faraday Discuss.*, 2015, **183**, 217–232.

90 G. R. Dey and S. Kamble, Effects of electrode material and frequency on carbon monoxide formation in carbon dioxide dielectric barrier discharge, *J. CO2 Util.*, 2020, **40**, 101207.

91 C. M. Mitsingas, R. Rajasegar, S. Hammack, H. Do and T. Lee, High Energy Efficiency Plasma Conversion of CO_2 at Atmospheric Pressure Using a Direct-Coupled Microwave Plasma System, *IEEE Trans. Plasma Sci.*, 2016, **44**, 651–656.

92 T. Nunnally, K. Gutsol, A. Rabinovich, A. Fridman, A. Gutsol and A. Kemoun, Dissociation of CO_2 in a low current gliding arc plasmatron, *J. Phys. D: Appl. Phys.*, 2011, **44**, 274009.

93 J.-Y. Wang, G.-G. Xia, A. Huang, S. L. Suib, Y. Hayashi and H. Matsumoto, CO_2 Decomposition Using Glow Discharge Plasmas, *J. Catal.*, 1999, **185**, 152–159.

94 T. Yong, H. Zhong, E. Pannier, C. Laux and M. A. Cappelli, High-pressure CO_2 dissociation with nanosecond pulsed discharges, *Plasma Sources Sci. Technol.*, 2023, **32**, 115012.

95 A. M. Banerjee, J. Billinger, K. J. Nordheden and F. J. J. Peeters, Conversion of CO2 in a packed-bed dielectric barrier discharge reactor, *J. Vac. Sci. Technol., A*, 2018, **36**, 04F403.

96 X. Duan, Z. Hu, Y. Li and B. Wang, Effect of dielectric packing materials on the decomposition of carbon dioxide using DBD microplasma reactor, *AIChE J.*, 2015, **61**, 898–903.

97 O. V. Golubev and A. L. Maximov, Dielectric Barrier Discharge Plasma Combined with Ce–Ni Mesoporous catalysts for CO_2 splitting to CO, *Plasma Chem. Plasma Process.*, 2024, **44**, 2087–2100.

98 J. Li, S. Zhu, K. Lu, C. Ma, D. Yang and F. Yu, CO_2 conversion in a coaxial dielectric barrier discharge plasma reactor in the presence of mixed ZrO_2–CeO_2, *J. Environ. Chem. Eng.*, 2021, **9**, 104654.

99 J. Li, X. Zhai, C. Ma, S. Zhu, F. Yu, B. Dai, G. Ge and D. Yang, DBD Plasma Combined with Different Foam Metal Electrodes for CO_2 Decomposition: Experimental Results and DFT Validations, *Nanomaterials*, 2019, **9**, 1595.

100 I. Michielsen, Y. Uytdenhouwen, J. Pype, B. Michielsen, J. Mertens, F. Reniers, V. Meynen and A. Bogaerts, CO_2 dissociation in a packed bed DBD reactor: First steps towards a better understanding of plasma catalysis, *Chem. Eng. J.*, 2017, **326**, 477–488.

101 Q. Yu, M. Kong, T. Liu, J. Fei and X. Zheng, Characteristics of the Decomposition of CO_2 in a Dielectric Packed-Bed Plasma Reactor, *Plasma Chem. Plasma Process.*, 2012, **32**, 153–163.

102 K. Zhang, G. Zhang, X. Liu, A. N. Phan and K. Luo, A Study on CO_2 Decomposition to CO and O_2 by the Combination of Catalysis and Dielectric-Barrier Discharges at Low Temperatures and Ambient Pressure, *Ind. Eng. Chem. Res.*, 2017, **56**, 3204–3216.

103 L. F. Spencer and A. D. Gallimore, Efficiency of CO_2 Dissociation in a Radio-Frequency Discharge, *Plasma Chem. Plasma Process.*, 2011, **31**, 79–89.

104 C. R. Nallapareddy and T. C. Underwood, What is "efficiency" in plasma chemical processes?, *iScience*, 2025, **28**, 112297.

105 Y. Itikawa, M. Hayashi, A. Ichimura, K. Onda, K. Sakimoto, K. Takayanagi, M. Nakamura, H. Nishimura and T. Takayanagi, Cross Sections for Collisions of Electrons and Photons with Nitrogen Molecules, *J. Phys. Chem. Ref. Data*, 1986, **15**, 985–1010.

106 H. Srour, A. Alnaboulsi, A. Astafan, E. Devers, J. Toufaily, T. Hamieh, L. Pinard and C. Batiot-Dupeyrat, Elimination of Coke in an Aged Hydrotreating Catalyst via a Non-Thermal Plasma Process: Comparison with a Coked Zeolite, *Catalysts*, 2019, **9**, 783.

107 H. Zhong, D. Piriaei, G. Liccardo, J. Kang, B. Wang, M. Cargnello and M. A. Cappelli, Cold plasma activated CO_2 desorption from calcium carbonate for carbon capture, *RSC Sustainability*, 2025, **3**, 973–982.

108 A. Logadottir, T. H. Rod, J. K. Nørskov, B. Hammer, S. Dahl and C. J. H. Jacobsen, The Brønsted–Evans–Polanyi Relation and the Volcano Plot for Ammonia Synthesis over Transition Metal Catalysts, *J. Catal.*, 2001, **197**, 229–231.

109 M. A. Signore, A. Della Torre, A. Serra, D. Manno, R. Rinaldi, M. Mazzeo, L. N. Francioso and L. Velardi, The Effect of Spark Current Tuning on the Formation of Cu Nanoparticles Synthesized by Spark Ablation in Nitrogen Atmosphere, *Crystals*, 2025, **15**, 587.

110 C. D. Wagner, *The NIST X-ray photoelectron spectroscopy (XPS) database*.

111 Z.-Q. Liang, T.-T. Zhuang, A. Seifitokaldani, J. Li, C.-W. Huang, C.-S. Tan, Y. Li, P. De Luna, C. T. Dinh, Y. Hu,

Q. Xiao, P.-L. Hsieh, Y. Wang, F. Li, R. Quintero-Bermudez, Y. Zhou, P. Chen, Y. Pang, S.-C. Lo, L.-J. Chen, H. Tan, Z. Xu, S. Zhao, D. Sinton and E. H. Sargent, Copper-on-nitride enhances the stable electrosynthesis of multi-carbon products from CO_2, *Nat. Commun.*, 2018, **9**, 3828.

112 N. H. Turner and J. A. Schreifels, Surface Analysis: X-ray Photoelectron Spectroscopy and Auger Electron Spectroscopy, *Anal. Chem.*, 1996, **68**, 309–332.

113 X. Fan, Z. Wu, H. Li, B. Geng, C. Li and P. Yan, Morphology and thermal stability of Ti-doped copper nitride films, *J. Phys. D: Appl. Phys.*, 2007, **40**, 3430–3435.